INL/JOU-20-58714-Revision-0

BISON: A Flexible Code for Advanced Simulation of the Performance of Multiple Nuclear Fuel Forms

March 2021

Changing the World's Energy Future

Richard L Williamson, Jason D Hales, Stephen R Novascone, Kyle A Gamble, Benjamin W Spencer, Wen Jiang, Stephanie A Pitts, Albert Casagranda, Daniel Schwen, Adam X Zabriskie, Aysenur Toptan, Russell Gardner, Christopher Matthews, Wenfeng Liu, Hailong Chen, Giovanni Pastore

INL/JOU-20-58714-Revision-0

BISON: A Flexible Code for Advanced Simulation of the Performance of Multiple Nuclear Fuel Forms

Richard L Williamson, Jason D Hales, Stephen R Novascone, Kyle A Gamble, Benjamin W Spencer, Wen Jiang, Stephanie A Pitts, Albert Casagranda, Daniel Schwen, Adam X Zabriskie, Aysenur Toptan, Russell Gardner, Christopher Matthews, Wenfeng Liu, Hailong Chen, Giovanni Pastore

March 2021

Idaho National Laboratory
Idaho Falls, Idaho 83415

http://www.inl.gov

Prepared for the
U.S. Department of Energy
Under DOE Idaho Operations Office
Contract DE-AC07-05ID14517

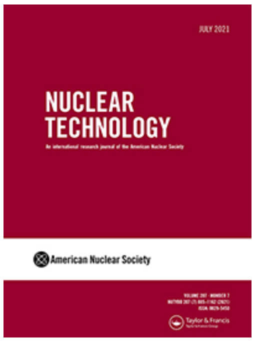

Nuclear Technology

ISSN: (Print) (Online) Journal homepage: https://www.tandfonline.com/loi/unct20

BISON: A Flexible Code for Advanced Simulation of the Performance of Multiple Nuclear Fuel Forms

Richard L. Williamson, Jason D. Hales, Stephen R. Novascone, Giovanni Pastore, Kyle A. Gamble, Benjamin W. Spencer, Wen Jiang, Stephanie A. Pitts, Albert Casagranda, Daniel Schwen, Adam X. Zabriskie, Aysenur Toptan, Russell Gardner, Christopher Matthews, Wenfeng Liu & Hailong Chen

To cite this article: Richard L. Williamson, Jason D. Hales, Stephen R. Novascone, Giovanni Pastore, Kyle A. Gamble, Benjamin W. Spencer, Wen Jiang, Stephanie A. Pitts, Albert Casagranda, Daniel Schwen, Adam X. Zabriskie, Aysenur Toptan, Russell Gardner, Christoper Matthews, Wenfeng Liu & Hailong Chen (2021) BISON: A Flexible Code for Advanced Simulation of the Performance of Multiple Nuclear Fuel Forms, Nuclear Technology, 207:7, 954-980, DOI: 10.1080/00295450.2020.1836940

To link to this article: https://doi.org/10.1080/00295450.2020.1836940

Published online: 20 Mar 2021.

NUCLEAR TECHNOLOGY · VOLUME 207 · 954–980 · JULY 2021
DOI: https://doi.org/10.1080/00295450.2020.1836940

Check for updates

BISON: A Flexible Code for Advanced Simulation of the Performance of Multiple Nuclear Fuel Forms

Richard L. Williamson,[a]* Jason D. Hales,[a] Stephen R. Novascone,[a] Giovanni Pastore,[a] Kyle A. Gamble,[a] Benjamin W. Spencer,[a] Wen Jiang,[a] Stephanie A. Pitts,[a] Albert Casagranda,[a] Daniel Schwen,[a] Adam X. Zabriskie,[a] Aysenur Toptan,[a] Russell Gardner,[b] Christoper Matthews,[c] Wenfeng Liu,[d] and Hailong Chen[e]

[a]*Idaho National Laboratory, Computational Mechanics & Materials Department, P.O. Box 1625, Idaho Falls, Idaho 83415*
[b]*Kairos Power, 707 W. Tower Avenue, Alameda, California 94501*
[c]*Los Alamos National Laboratory, Materials Science in Radiation and Dynamics Extremes, Los Alamos, New Mexico 87545*
[d]*Structural Integrity Associates Inc., 9710 Scranton Road, Suite 300, San Diego, California 92121*
[e]*University of Kentucky, 185 Ralph G. Anderson Building, Lexington, Kentucky 40506-0503*

Received July 10, 2020
Accepted for Publication October 12, 2020

Abstract — *BISON is a nuclear fuel performance application built using the Multiphysics Object-Oriented Simulation Environment (MOOSE) finite element library. One of its major goals is to have a great amount of flexibility in how it is used, including in the types of fuel it can analyze, the geometry of the fuel being modeled, the modeling approach employed, and the dimensionality and size of the models. Fuel forms that can be modeled include standard light water reactor fuel, emerging light water reactor fuels, tri-structural isotropic fuel particles, and metallic fuels. BISON is a platform for research in nuclear fuel performance modeling while simultaneously serving as a tool for the analysis of nuclear fuel designs. Recent research in BISON includes techniques such as the extended finite element method for fuel cracking, exploration of high-burnup light water reactor fuel behavior, swelling behavior of metallic fuels, and central void formation in mixed-oxide fuel. BISON includes integrated documentation for each of its capabilities, follows rigorous software quality assurance procedures, and has a growing set of rigorous verification and validation tests.*

Keywords — *Finite element, BISON, MOOSE.*

Note — *Some figures may be in color only in the electronic version.*

I. INTRODUCTION

Nuclear fuel performance modeling is used for a variety of purposes, including fuel design and optimization, experiment planning and interpretation, and operational and safety analysis. Such modeling is typically performed using dedicated fuel performance codes, a number of which have been developed for specific fuel types. Fuel vendors, utilities, safety authorities, and research organizations develop or use these codes to predict the behavior and lifetime of fuel during standard operation, accidental transients, and post-irradiation storage. A comprehensive review of nuclear fuel performance modeling was recently published.[1]

*E-mail: richard.williamson@inl.gov

Nuclear fuel operates in extreme environments that induce complex coupled physics phenomena occurring over distances ranging from inter-atomic spacing to meters, and timescales ranging from microseconds to years. This multiphysics behavior is often tightly coupled, a well-known example being the thermomechanical behavior during final gap closure in light water reactor (LWR) fuel rods. In addition, many important aspects of fuel behavior are inherently multidimensional, such as cladding ballooning in LWR fuel, fracture of the layers that comprise tri-structural isotropic (TRISO) particle fuel, and anisotropic swelling in metallic fuel.

Since 2008, Idaho National Laboratory (INL) has been developing next-generation capabilities to model nuclear fuel behavior, resulting in the BISON finite element fuels code.[2] BISON is based on the Multiphysics Object-Oriented Simulation Environment (MOOSE) computational framework,[3] and from the beginning was designed to be "multi" in several aspects, including multiphysics, multidimensional, multiscale, and multifuel. With regard to multiphysics, the BISON governing relations currently consist of nonlinear partial differential equations for energy, species, and momentum conservation, and can be solved either fully or loosely coupled. BISON supports a variety of geometries, providing one-dimensional (1-D) (spherical or layered), two-dimensional (2-D) (axisymmetric, Cartesian, or layered), and full three-dimensional (3-D) analysis capabilities. BISON was developed and is used in close coordination with meso- and atomistic-scale codes and analyses, providing lower-length-scale-informed models for complex material behavior. Finally, BISON was designed to analyze a variety of fuel types, including standard and emerging LWR fuel concepts, TRISO particle fuel, and metallic fuels. The code was developed with flexibility as a goal, including a programming structure that readily permits the addition of enhanced capabilities (such as a new material model) and the ability to run on a laptop computer or large cluster.

Following early fuel performance prototyping using commercial finite element software,[4] BISON development for LWR and TRISO particle fuel began in earnest in 2009 and was first reported in 2012 (Ref. 2). Further development and benchmarking of BISON for TRISO fuel was published in Ref. 5. Continuous code verification has been a priority during the development process, as outlined in Ref. 6. As LWR capabilities matured, a significant code validation effort ensued, first documented in Ref. 7. That effort continues today. Extensive development and early validation of BISON for metallic fuel has been accomplished in recent years and will be published shortly. Numerous other articles and reports, many summarized herein, document the development, application, verification, and validation of BISON throughout the last decade.

The objective of this paper is to outline the current status of BISON, including a variety of examples that demonstrate important, and in many cases, novel capabilities. Much like a review paper, descriptions will be relatively high level, relying on referenced literature for details.

This paper begins with an overview of foundational capabilities, including descriptions of the MOOSE multiphysics finite element framework, integrated code, and validation documentation, and software quality assurance (SQA). The next five sections outline the capability to analyze specific fuel types, namely, LWR fuel, advanced technology LWR fuel, TRISO particle fuel, metallic fuel, and finally, void formation in mixed-oxide (MOX) fuel. A description of BISON verification and validation follows, concluding with a description of current and future development directions.

II. FOUNDATIONAL CAPABILITIES

The MOOSE framework, on which BISON is built, provides the core functionality needed to solve coupled physics field equations with the finite element method.[3] Generic capabilities to solve the various types of physics, including the heat transfer, mechanics, and contact capabilities used within BISON simulations, are provided by the MOOSE physics modules. MOOSE also provides built-in capabilities for parallel coupled multiscale solves through its `MultiApp and Transfer` systems. BISON uses the thermomechanical capabilities of MOOSE in combination with nuclear-specific material and physics models to simulate a variety of fuel forms. The primary MOOSE framework capabilities used by BISON are described herein.

II.A. Multidimensional Multiphysics Finite Element Framework

BISON solves the multiphysics problems inherent in fuel performance analysis by solving the fully coupled nonlinear partial differential equations for thermomechanics.[8] In addition, BISON has the capability to solve simulations on multiple length scales, different dimensions, and as part of a coupled simulation with other codes. This versatility allows BISON to increase modeling fidelity or emphasize computational efficiency, depending on the simulation requirements.

The ability to simulate fuel performance behavior through multiscale information passing enables higher-fidelity modeling in BISON (Ref. 9). Lower-length-scale work allows for improvements on classical empirical models of fuel performance, particularly in the area of metallic fuel modeling.[10,11] Discussed in Sec. VI.D, these lower length scales improve the simulation of engineering-scale fuel performance through the creation of physics-informed models.

BISON supports multidimensional simulations that solve the fully coupled nonlinear partial differential equations involved in nuclear fuel performance modeling. This capability uniquely positions BISON to model phenomena of interest to the LWR fuel performance community, including pellet-cladding mechanical interaction (PCMI) behavior induced by missing pellet surface (MPS) defects.[12–14] BISON has been used to study the influence of an MPS defect on the mechanical response of the cladding.[15] In a similar application, the 3-D functionality of BISON was harnessed to aid in planning an experiment in the Halden Research Reactor for validating MPS defect simulations and to investigate the role of the MPS defect size on the measurable cladding deformation.[16] The 3-D modeling capabilities of BISON enabled the successful simulation of these localized geometry defects. Additional multidimensional modeling efforts in BISON are discussed in Secs. V.C and VII.A.

In recent years, a low-dimensional capability, termed layered 1-D or 1.5-D, has been added to BISON. The layered 1-D modeling capability consists of several rows of line elements arranged axially in slices to represent a fuel rod.[17] On each slice of the radial line elements, a 1-D model of the physics (energy conservation, stress divergence, thermal and mechanical contact) is solved. The mechanical interaction between these line elements is coupled in the axial direction with a specifically developed generalized plane-strain capability that transfers a homogeneous scalar general strain between axially adjacent line elements. A similarly termed layered 2-D capability models the axial position slices using 2-D Cartesian meshes. The extension of the layered 1-D capability to the layered 2-D functionality enables the introduction of azimuthal variation in the boundary conditions.[18]

A series of comparisons between layered 1-D and 2-D axisymmetric simulations of a set of validation cases was performed to assess the layered 1-D capability.[19] As a low-dimensional simulation, this layered 1-D capability is unable to accurately replicate the stress and strain predictions of the 2-D and 3-D BISON simulations. However, the layered 1-D capability excels in computational efficiency: A simulation runtime reduction of one to two orders of magnitude was routinely observed. The computational efficiency of the layered 1-D capability would lend itself well to a scoping study to identify parameters of interest, such as for a fuel rod in which a high stress state occurs. Once the rods of interest are identified, a higher-dimension study can be run on just those rods.

The computational efficiency of the layered 1-D simulations can also enable the coupling of BISON with other simulation codes. In a coupled quarter-core nuclear reactor simulation based on Watts Bar Nuclear Plant Unit 1 (cycle 1), the reduced geometric complexity of the layered 1-D BISON capability enabled the tight coupling of BISON with the neutron transport [e.g., MPACT (Ref. 20)] and thermal hydraulics [e.g., CTF (Ref. 21)] codes, through the Virtual Environment for Reactor Applications (VERA) used in the simulations reported in Ref. 22. This simulation demonstrates the high-fidelity coupled methodology that may potentially be required to successfully model transient cases on the scale of a reactor core.

The flexibility of simulation and multicode coupling afforded by the MOOSE framework have been of growing interest to academic and industry partners alike. The U.S. Nuclear Regulatory Commission (NRC) proposed using the MOOSE coupling approach to couple legacy NRC codes to advanced modeling tools currently under development through the U.S. Department of Energy (DOE) for confirmatory analysis. The concept is known as the Comprehensive Reactor Analysis Bundle (CRAB). Through the use of a MOOSE-wrapped application, a code that is external to MOOSE can be treated as a native MOOSE application, allowing the non-native code to leverage all of MOOSE's capabilities. A coupling demonstration was completed as a proof of concept for CRAB. For this demonstration, BISON was coupled to the NRC's legacy thermal-hydraulic system code TRACE to allow thermomechanical phenomena feedback between the fuel rod and reactor coolant. The Loss of Fluid Test (LOFT) L2-5 experiment was recommended by the NRC as a first validation case, as test data and TRACE code inputs were already available. The LOFT experiments were designed to test the system response during a loss-of-coolant accident (LOCA) and presented a challenging experiment to simulate. Fully coupled simulations with CRAB were completed, with results demonstrating clear improvement over calculations made using TRACE alone.[23,24]

II.B. Integrated Documentation

As with any finite element analysis software, the accessibility of BISON is determined in part by the quality of the code documentation. Documentation is a key method of communicating BISON's modeling capabilities to current and potential users. The BISON documentation system in prior years[2] used static PDF user and theory manuals. These static manuals could easily become out of date with respect to the source code and required significant effort to maintain. In the last few years, a new web-based, dynamic BISON documentation system has been implemented.[25,26] This BISON documentation approach, built on the MooseDocs system,[27,28] is tightly integrated with the BISON source code, thereby ensuring real-time documentation updates.

Cohesive and simultaneous development of the documentation along with the BISON source code is the defining principle of the web-based BISON documentation system. Use-case examples for each code element are linked directly from BISON regression, verification, and validation input files, ensuring that the documentation examples reflect the current BISON code state. Documentation standards were developed to outline content and format expectations with the goal of presenting a consistent, uniform interface to users. The MooseDocs system includes the functionality to directly link to the source code test design requirements within a requirement's traceability matrix[28] as part of the BISON documentation system.[29] This matrix is one of the elements of the SQA process discussed in Sec. II.C. Strict requirements for documentation coverage are enforced by the automatic testing system prior to acceptance of any source code change.

Development of the documentation navigation experience focused on accommodating a wide range of user experience levels. Quick links, search functionality, and curated table-of-contents lists allow advanced users to rapidly find a specific documentation page. For new users, guided step-by-step instructions with copy-read example commands are provided to help download and build BISON. Detailed descriptions of simplified LWR examples are included with links to many BISON code elements. Descriptions of the BISON validation cases are incorporated into the web-based documentation system. Detailed descriptions of the material models applied in these validation cases are given as links to the relevant documentation pages. Such integration allows users to quickly explore the different material models used in each validation analysis.

The official BISON documentation website is built daily from the BISON code repository and reflects the current BISON source code state. Functionality within the MooseDocs system allows a local build of the documentation system based on the user's locally built version of BISON, thereby ensuring a direct match between the local BISON code and the local documentation.

II.C. Software Quality Assurance

BISON follows a SQA procedure aligned with American Society of Mechanical Engineers' (ASME's) Nuclear Quality Assurance-1 (NQA-1) requirements. The use of ASME's NQA-1 standard is endorsed by the NRC and is therefore a key requirement for fuel performance analysis software used in license applications.

BISON development procedures include, among other things, issue tracking, version control, peer review, regression testing, testing, and quantification of code coverage.[6,30] These procedures are flexible enough to accommodate the modern agile software development process while tracking, through the MooseDocs system, the software design requirements and accompanying documentation for each code element. Two separate reviews are completed before a source code change is accepted into BISON: an independent code review of the individual code change and a technical lead review when a version of BISON is given an official version tag.

III. LWR FUEL

In this section, we summarize BISON capabilities and applications for modeling LWR fuel rod behavior. Initially, BISON development, verification, and validation for LWR fuel was focused on behavior under normal reactor operating conditions and power ramps.[2,6,7] More recently, code development and validation work for the analysis of design-basis accidents such as LOCA and reactivity-initiated accident (RIA) scenarios has been performed.[23,31–36]

Hereafter, we provide summary descriptions and references for the BISON capability status and applications to LWR fuel modeling.

III.A. Material and Behavioral Models

Basic descriptions of the models incorporated into BISON to predict UO_2-Zircaloy LWR fuel performance are outlined in Secs. III.A.1 and III.A.2.

III.A.1. Base Models

The thermal conductivity of UO_2 fuel is calculated using the model from Ref. 37. To capture the radial power distribution in the fuel during irradiation, a model based on Refs. 38 and 39 is used. To represent the effect of fuel cracking, multiple models of varying complexity are available in BISON, including an orthotropic smeared cracking model[40] and a simple isotropic softening model,[41] as well as advanced techniques described in Sec. III.C. MATPRO models are used for fuel creep and solid fission product swelling.[42] A modified ESCORE model is used for fuel densification.[43] Gaseous fission product swelling and fission gas release (FGR) are computed by a physics-based model from Refs. 44 and 45. Grain growth is calculated using the model from Ref. 46.

For pellet-fragment relocation, the empirical ESCORE model[47] is applied; this model was calibrated by Swiler et al.[48] for use in BISON.

The BISON models for Zircaloy-2/4 thermal and irradiation creep at normal operating temperatures were given by Limbäck and Andersson.[49] The model for irradiation growth of Zircaloy cladding is the one developed by Franklin.[50] To treat mechanical contact between the fuel and the cladding, BISON uses an approach based on the methodology of Heinstein and Laursen.[51] The conductance of the fuel-to-cladding gap can be calculated using the legacy gap conductance modeling[52–54] and the improved gap conductance modeling.[55–58]

III.A.2. Models for Accident Conditions

Axial relocation of fuel fragments during postulated LOCA accidents is accounted for in BISON using a semi-empirical model originally developed by Jernkvist and Massih.[59] BISON capabilities for Zircaloy cladding analysis under LOCA conditions include models for high-temperature oxidation from Ref. 60, crystallographic phase transition based on Ref. 61, high-temperature creep from Ref. 62, and failure due to burst based on Refs. 62 and 63.

A Zircaloy plasticity model applicable at high temperatures and strain rates[64] was implemented in BISON. This model has been successfully used to simulate the Organisation for Economic Co-operation and Development RIA benchmark cases, as described in Ref. 32. Also, a transient fission gas behavior model that accounts for the effect of fuel micro cracking in FGR is available.[65,66] This transient model has been applied in BISON simulations of RIA tests, demonstrating an improved predictive capability for FGR during RIA compared to traditional models.[33]

III.B. Overview of Applications

BISON has been applied to the simulation of a variety of LWR fuel problems encompassing fuel rod irradiation experiments under normal operating conditions and power ramps,[7] LOCA experiments including both separate-effects cladding ballooning tests and integral fuel rod tests,[23,31,35,36] RIA experiments,[32,34,67] and idealized problems involving specific multidimensional aspects such as MPS fabrication defects.[15,68,69] As mentioned previously, BISON has been coupled to the MPACT (neutronics) and CTF (thermal hydraulics) codes through VERA, and in one application[70,71] was used to perform quarter-core simulations of all fuel rods to identify specific rods most susceptible to PCMI failure. These cases demonstrate the code's ability to simulate various aspects of fuel rod behavior, including thermal response, FGR, and mechanical behavior such as cladding elongation, PCMI, cladding ballooning, and burst failure.

Many of the BISON LWR experimental validation cases grew out of INL's participation in the International Atomic Energy Agency's (IAEA) Coordinated Research Projects FUMEX-II (Ref. 72), FUMEX-III (Ref. 73), and FUMAC (Ref. 74). A more detailed account of BISON validation to LWR fuel experiments is given in Sec. VIII.

While most BISON applications for integral LWR fuel rod analysis used 2-D geometrical representations, the multidimensional modeling capability of BISON implies the potential to investigate inherently 3-D aspects. One example is analyzing the effect of fuel pellet eccentricity (radial offset) on the radial temperature distribution in the fuel, previously demonstrated through the simulation of the Halden test Instrumented Fuel Assembly-431 (IFA-431) (Ref. 7). Another important 3-D application of BISON concerns the analysis of local geometric irregularities, particularly MPS defects. Such an application was demonstrated in Ref. 15, where BISON's 3-D capability was used to simulate the local fuel rod response in the MPS region for a boiling water reactor (BWR) fuel rod subject to a variety of transient events. The analysis involved a 3-D model of the region of the fuel rod containing the MPS coupled to a 2-D full-length rod model for calculating integral quantities. Results demonstrated the ability to explicitly capture the MPS effects on the local thermomechanical fuel rod behavior, including during PCMI. Figure 1 shows typical results from that analysis, with full details provided in Ref. 15. Finally, under LOCA conditions, 3-D aspects such as the effects of azimuthal temperature variations in the cladding can be important in affecting the cladding ballooning and burst behavior. A 3-D analysis of a LOCA cladding test that included azimuthal temperature variations, presented in Ref. 35, demonstrates the nonuniform cladding ballooning along with a localized burst, consistent with the experimental observations[75] reproduced by BISON.

III.C. Fracture Modeling

While fracture in LWR fuel is not generally a direct safety concern, it has important impacts on the performance of LWR fuel during normal operation, including having a major influence on the fuel stress state, being a major contributor to radial fuel relocation, influencing the effective thermal conductivity of the fuel, and creating local stress concentrations in the cladding adjacent to

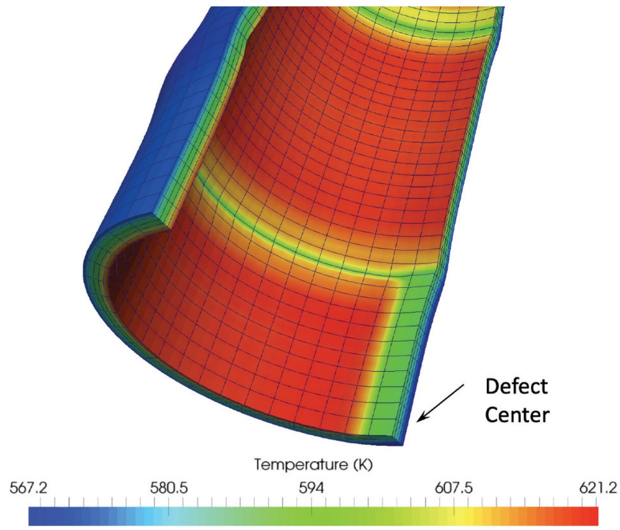

(a)

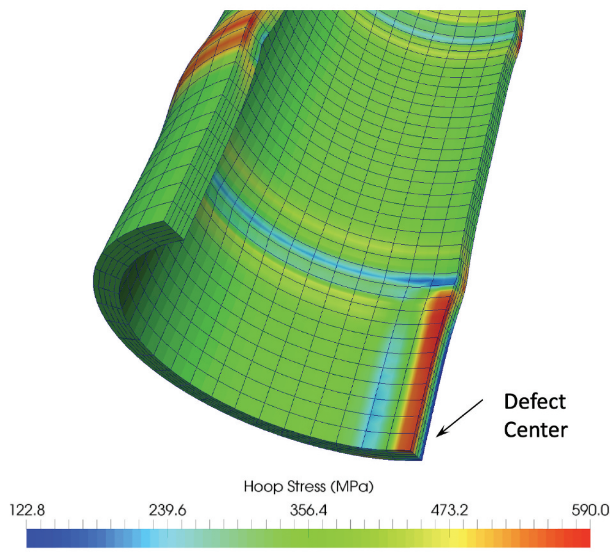

(b)

Fig. 1. (a) Computed temperature and (b) hoop stress in the cladding near an MPS defect. The localized reduction in cladding temperature and substantial increase in hoop stress can only be accurately computed using 3-D analysis.

cracks. During accident conditions, the size distribution of fuel fragments affects the way they are dispersed in the coolant in the event of a cladding rupture. Since its early development, BISON featured smeared cracking models that allow it to account for the effects of cracking on the stress state of the fuel, but which are limited in their ability to predict the formation of discrete cracks or fragments.

Efforts have been underway to incorporate state-of-the-art fracture modeling techniques into BISON to allow for a more physics-based representation of fracture propagation and its effects on fuel performance. These have primarily focused on the extended finite element method (`XFEM`) and peridynamics.

The extended finite element method allows for arbitrary evolving discontinuities to be represented in a finite element simulation independent of the underlying finite element mesh. These discontinuities can be used to represent cracks as discontinuities in the displacement field, but can also be used to represent other types of discrete discontinuities that occur in multiphysics simulations, such as an interface between two materials. The MOOSE `xfem` module uses the phantom node technique to implement `XFEM` solution field enrichment and has been documented in detail and demonstrated for 2-D nuclear fuel fracture.[76]

Peridynamics is a mesh-free technique for modeling field equations that uses integral rather than differential equations. It satisfies equilibrium through a set of interactions between material points and their neighbors that fall within a specified radius, known as a horizon. The bonds that represent connections between these material points can be removed when a local fracture criterion is reached, allowing for fracture and fragmentation to be represented in an unguided manner. This has been implemented in the MOOSE `peridynamics` module and has been applied to fuel fracture.[77]

In addition to the development of these new fracture techniques, the ability of the existing smeared cracking technique to model the formation of individual cracks has recently been enhanced through the use of a volume-weighted fracture strength randomization technique that enables it to better capture fracture localization.

Figure 2 shows a comparison of predicted fracture patterns and temperature fields in fresh LWR fuel after a ramp up to full power using `XFEM`, peridynamics, and smeared cracking. Each technique has its own advantages and disadvantages, and all are useful for addressing various aspects of fuel fracture and its effects.

IV. ADVANCED TECHNOLOGY FUEL

IV.A. Background

Advanced technology fuel (ATF) concepts, formerly known as accident-tolerant fuel concepts, are fuel and cladding materials proposed to improve response time in the event of an accident (e.g., LOCA, RIA), and at the same time maintain equal or improved performance

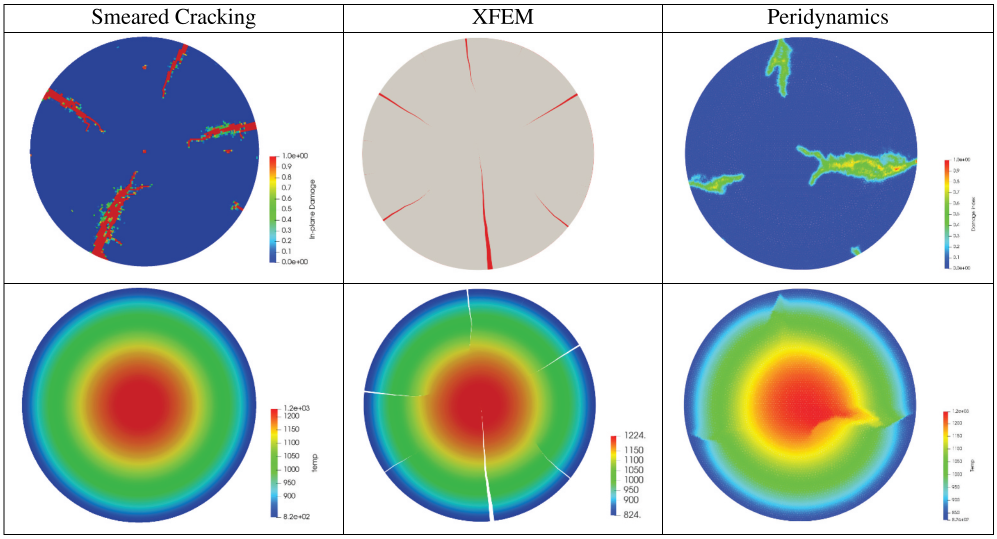

Fig. 2. Comparison of temperature fields and radial crack patterns predicted in an LWR fuel cross-section model using (a) smeared cracking, (b) `xfem`, and (c) peridynamics. (top row) Damage fields (and discrete crack locations in the case of `xfem`) and (bottom row) temperature fields (in kelvins) are shown.

during normal operation.[78] Intense research into these concepts by national laboratories, universities, and industry began after the events that occurred at the Fukushima Daiichi nuclear power plant in 2011.

From a cladding perspective, concepts were selected that potentially mitigate the rapid oxidation of the existing Zircaloy-based cladding during accidents, which was the cause of the hydrogen explosions at Fukushima. For fuels, the primary focus has been to increase thermal conductivity to lower the fuel's operating temperature and reduce the amount of FGR. An added benefit of many of the fuel concepts is the higher uranium loading for improved economics compared to traditional UO_2.

In BISON, capabilities have been added to model U_3Si_2 and Cr_2O_3-doped fuel, as well as iron-chromium-aluminum (FeCrAl) and Cr-coated Zircaloy claddings. The approach has been to stand up an initial empirical capability while identifying the range of applicability and uncertainty in the models. Then, for material and behavior models with limited or no experimental material property data, utilize a multiscale modeling approach.[79–81] A summary of the models available in BISON for each ATF concept and the studies completed on them are summarized in Secs. IV.B through IV.F.

IV.B. U_3Si_2 Fuel

Westinghouse has pursued U_3Si_2 fuel as an ATF concept for its higher thermal conductivity and uranium density as compared to UO_2. At the time of conception, concerns regarding the use of U_3Si_2 in LWRs included the potential for uncontrollable swelling (as seen at research reactor temperatures) and the possibility of it dissolving in water after a cladding breach. Through multiscale modeling approaches, it was determined that uncontrollable gaseous fission product swelling was not expected during operation at LWR temperatures.[82,83]

Models have been incorporated into BISON for thermal conductivity and its degradation,[82,84] specific heat,[84] Young's modulus,[84] Poisson's ratio,[84] thermal creep,[85] solid swelling,[86] and FGR and gaseous swelling.[83] Further refinements to the FGR and thermal creep models through multiscale modeling approaches are underway.

BISON has been used to analyze two U_3Si_2-fueled rods (ATF-13 and ATF-15) that underwent post-irradiation examination[87] following irradiation in the Advanced Test Reactor at INL. By incorporating sensitivity analysis and uncertainty quantification, it was found that simulation predictions bound the limited available experimental data.[81]

BISON has been used to evaluate the performance of U_3Si_2 fuel in several recent applications. In Refs. 88 and 89 the code was used to investigate the proposed U_3Si_2-SiC fuel cladding concept during normal operation, and then extended to power ramps and RIA conditions in Ref. 89. Very recently, BISON was used to compare the behavior of Zircaloy-clad UO_2 and U_3Si_2 under normal operation, and then extended to demonstrate how varying thermodynamic and chemical kinetics influence fuel expansion and subsequent cladding performance during a cladding breach.[90] In an interesting application of BISON's multidimensional capabilities, these simulations were further extended to a 3-D fuel rod subsection to demonstrate the characteristics of the resulting cladding crack.

IV.C. Cr_2O_3-Doped UO_2 Fuel

Westinghouse, Framatome, and Global Nuclear Fuel (GNF) are exploring Cr_2O_3-doped UO_2 fuel as an ATF concept due its larger grain size and potential reduction of FGR and rod internal pressure. It is unclear how the larger-grain-sized fuel will affect the thermophysical properties. Currently, except for the initial grain size and the FGR and gaseous swelling model for Cr_2O_3-doped UO_2, all other models (i.e., thermophysical properties, solid swelling, and densification) are assumed to be the same as UO_2 (Ref. 7).

The Cr_2O_3-doped UO_2 capabilities in BISON have been validated to the IFA-677 and IFA-716 experiments irradiated at the Halden reactor in Norway, as well as the AREVA ramp tests.[91] Validation to these experiments has demonstrated the usefulness and importance of multiscale modeling.[81]

As an initial application of BISON's Cr_2O_3-doped UO_2 capabilities, in Ref. 91 a large-break LOCA case was simulated, providing an initial assessment of the enhanced safety associated with chromia-doped fuel as compared to standard UO_2 fuel in LWRs.

IV.D. FeCrAl Cladding

The concept of FeCrAl is under consideration by GNF and has been primarily developed by Oak Ridge National Laboratory (ORNL) to replace the existing Zircaloy-based cladding due to FeCrAl's improved oxidation resistance[92] and strength.[93] Because of its higher thermal neutron absorption cross section, FeCrAl claddings must be thinner. This reduction in cladding thickness allows for slightly larger pellets to maintain the same cold gap width of the fuel rod. However, the slight increase in pellet diameter is not sufficient to compensate for the neutronic penalty, and enriching the fuel beyond the current 5% limit appears necessary.[94] Current estimates indicate that this neutronic penalty will impose an increase in fuel cost of 15% to 35% (Ref. 95). Tritium release is also of concern for FeCrAl (Ref. 96).

In BISON, models exist for failure,[97] thermal creep,[98] irradiation swelling,[98] Young's modulus and Poisson's ratio,[93] thermal expansion,[99] thermal conductivity and specific heat,[99] tritium permeability,[96] and oxidation.[92] Some of the models are specific to four different FeCrAl alloys: APMT, C06M, C35M, and C36M.

Several related studies have used BISON to perform fuel performance evaluations of FeCrAl claddings under normal LWR operating conditions.[100–103] These studies considered both commercially available alloys[101–103] and new FeCrAl alloys under current development.[103] Collectively, these investigations provide an important summary of the advantages and disadvantages of FeCrAl alloys in comparison to current Zr-based cladding.

BISON has also been used for qualitative comparisons to Zircaloy-4 in burst tests for which the experimental conditions were known. It was found that Zircaloy-4 and FeCrAl exhibited similar behavior, given the necessity to reduce the cladding thickness.[80,97]

IV.E. Cr-Coated Cladding

The addition of pure chromium on the waterside surface of Zircaloy-based claddings is to reduce oxidation and the subsequent production of hydrogen. All fuel vendors have a Cr-coated concept. The material models available for pure chromium in BISON were first compiled by Ref. 104, including creep, Young's modulus, Poisson's ratio, thermal expansion, thermal conductivity, specific heat, oxidation, and yield stress (plasticity). Initial normal operation comparisons to uncoated Zircaloy-based tubes completed by Ref. 104 illustrated comparable behavior. BISON was also used in conjunction with an experimental assessment of the feasibility of using cold spray techniques to apply Cr-coatings, concluding that the concept has high potential benefits but requires further optimization and testing.[105]

The BISON chromium models have also been used in a parametric numerical experiment to confirm the postulated claim that coated cladding tubes balloon less during LOCA-like conditions than uncoated tubes, thus resulting in a more coolable geometry.[106]

IV.F. Additional ATF Applications

BISON has also been utilized to evaluate other ATF concepts and materials.

One fuel concept proposes the use of conductive molybdenum inserts, either disks placed between standard UO_2 fuel pellets or finned structures embedded within pellets, to reduce fuel temperatures. Computational feasibility studies with BISON (in three dimensions) indicated substantial temperature reductions are achievable using either of these conductive inserts, suggesting further experimental and computational studies are warranted.[107]

Multimetallic layered composite (MMLC) cladding is a recently proposed concept designed to provide improved fuel rod survivability during LWR accident scenarios.

BISON has been used to evaluate the mechanical performance of MMLC cladding using both small-scale and full-length rod simulations, with parametric studies used to provide cladding design recommendations.[108]

BISON's basic thermomechanic capabilities have also been used to study SiC-SiC composite materials for both cladding and channel box applications. In Refs. 109 and 110, parametric studies of SiC-SiC composite cladding are used to evaluate the interaction of the fuel and cladding under differing initial gap and power conditions, including the impact of a nonuniform power profile. In Refs. 111 and 112, BISON was used to study the deformation behavior of proposed SiC-SiC composite channel box core components under expected BWR neutron flux and temperature distributions.

V. TRISO PARTICLE FUEL

V.A. Background

Researchers have studied TRISO fuel particles for use in high-temperature, gas-cooled reactors, though their use in other reactor types is now drawing interest. These particles are roughly 1 mm in diameter and consist of a fuel kernel (UO_2 or UCO), a graphite buffer layer, an inner pyrolytic carbon (IPyC) layer, a SiC layer that acts as the primary fission product barrier, and an outer pyrolytic carbon (OPyC) layer. Analysis of TRISO particles typically assumes spherical symmetry. However, multidimensional effects can be important.[5]

V.B. Material and Behavioral Models

Table I summarizes the solution scheme, applicable particle geometries, and the material and behavioral models currently available for TRISO particle fuel analyses using BISON. These capabilities are documented in greater detail in Ref. 29.

V.C. Multidimensional TRISO Demonstration

Cracking of the IPyC layer is a typical failure mode observed in post-irradiation examination of fuel particles.[113] During irradiation, shrinkage of the pyrocarbon (PyC) layers causes significant tensile stress in those layers. If the stress exceeds the tensile strength of that material, a radial crack forms in that PyC layer. The radial crack leads to a high local tensile stress in the SiC layer adjacent to the cracked PyC layer, potentially leading to particle failure. To model the cracking behavior, the extended finite element method is used to represent discrete cracks in the BISON TRISO particle model. Figure 3a shows a 2-D axisymmetric model in which a radial crack cuts through the thickness of the IPyC layer. Due to axisymmetry, the crack effectively extends around the full circumference of the particle. Figure 3a shows a 3-D one-eighth symmetric model in which

TABLE I

Summary of BISON TRISO Fuel Performance Models

Feature	Summary
Solution scheme	Finite element: massively parallel, coupled nonlinear partial differential equations (heat conduction, mechanics, fission product species transport), fully implicit
Geometry	Supports 1-D spherical, 2-D axisymmetric, and 3-D
Material models[a]	Kernel: UO_2 and UCO, solid and gas swelling, densification, thermal expansion; buffer: isotropic irradiation strain, irradiation creep, thermal expansion
	PyC: anisotropic irradiation strain, irradiation creep, thermal expansion; and SiC: irradiation creep, thermal expansion
Gap behavior	Gap between buffer and IPyC: heat transfer, mass transfer, and mechanical contact
Fission products modeling	FGR: physics-based model[44] for UO_2 and Recoil-Booth model for UCO, fission product diffusion
Failure modeling	Failure probability calculation using Monte Carlo; failure mechanisms can be modeled[b]: pressure vessel failure, IPyC cracking, debonding, asphericity, SiC thinning, SiC thermal decomposition, SiC palladium penetration, kernel migration

[a]All material models from the PARFUME fuel performance code have been implemented in BISON.
[b]BISON has the capability to model these failure phenomena in multiple dimensions, however, the failure modes currently used in Monte Carlo simulation are pressure vessel failure, IPyC cracking, and asphericity. The work to incorporate all those failure modes is under active development.

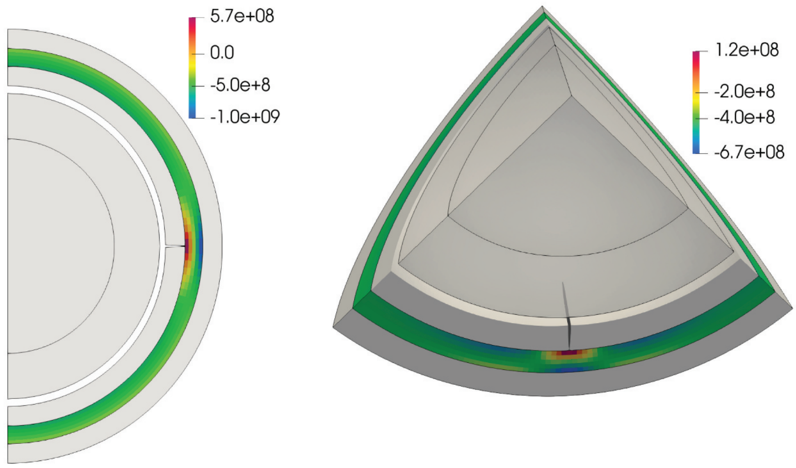

(a) 2D axisymmetric model. (b) 3D one-eighth symmetric model.

Fig. 3. BISON IPyC cracking model: contour plot of the tangential stress (in pascal) of SiC layer at 3×10^6 s.

a radial crack with a length of 0.1 mm cuts through the thickness of the IPyC layer. Due to eighth-symmetry, it is equivalent to modeling four radial cracks with a length of 0.2 mm in a complete spherical model.

As can be seen in Figs. 3a and 3b, the presence of an IPyC crack leads to a stress concentration in the SiC layer in the vicinity of the crack tip. Figure 4 plots the tangential stress histories in the SiC layer at a point near the crack tip for both intact and cracked particles. Contrary to the stress history for an intact particle, the tangential stress near the crack tip quickly becomes tensile, rising to a peak value of 580 and 120 MPa for two dimensions and three dimensions, respectively. The difference in peak value highlights the importance of enabling an evaluation of multidimensional effects. After reaching the peak, the stress is eventually relieved due to creep in the PyC layers.

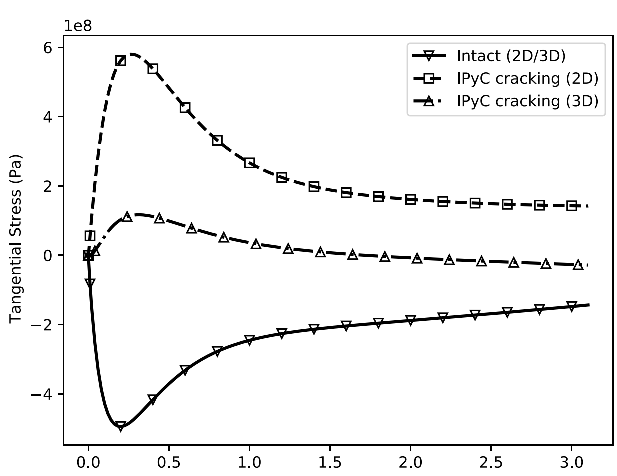

Fig. 4. Tangential stress histories at the inner surface of SiC near the crack tip.

V.D. Recent Applications

BISON has recently been employed in a variety of TRISO particle fuel investigations, including simulation of the thermomechanical behavior of fuel particles in fully ceramic microencapsulated (FCM) fuel irradiated under prototypic LWR conditions,[114] analysis of stress evolution in fuel particles containing novel composite architectures for both the SiC and PyC layers,[115] calculation of radionuclide release from particle fuel during post-irradiation annealing (including comparison to experimental data),[116] and simulation of the thermomechanical and failure behavior of fuel particles subjected to transient power pulse conditions in the Nuclear Safety Research Reactor[117] (NSRR).

VI. METALLIC FUEL

VI.A. Background

Due to their inherent safety and reprocessing capability, zirconium-based metallic fuels such as U-Zr and U-Pu-Zr have been used in nuclear reactors since the early days of nuclear energy, with the Experimental Breeder Reactor (EBR) program being a prime example.[118,119] EBR-II operated for approximately 30 years (1964 to 1994) and accomplished several important objectives related to sodium-cooled fast reactors and metallic fuels.

ANS

EBR-II demonstrated that a closed fuel cycle using metallic fuel was possible, and by 1969 ~35 000 fuel pins had been successfully reprocessed, refabricated, and reinserted into the reactor. Many important experiments were performed in the reactor, and significant advances in materials were made over this time. Eventually, burnups of ~20% were reached in EBR-II using a U-Pu-Zr fuel composition combined with HT9 cladding. Finally, in the later years of EBR-II operation, the reactor was used to demonstrate the integral fast reactor concept. Both a loss-of-flow and a loss-of-heat-sink accident were performed at EBR-II in 1986. During each accident, no operator intervention was required, and the reactor passively shut down.

The behavior of metallic fuels is complex and depends on composition, porosity, temperature, and other factors.[120] In recent years, BISON has been updated to account for these phenomena and to provide accurate simulations of zirconium-based metallic fuel in fast reactors.[121] BISON has recently been used to evaluate the fuel performance of annular metallic fuels for an advanced fast reactor concept[122] and is currently being used for fuel design studies for the Versatile Test Reactor.[123]

The requisite material models to accurately represent complex metallic fuel behavior are thermal conductivity, heat capacity, thermal expansion, mechanical elasticity, thermal and irradiation creep, solid and gaseous fission product swelling with corresponding porosity generation and interconnection, and zirconium redistribution.

Cladding material models consist of basic thermomechanic models for three variations of stainless steel: 316, D9, and HT9. In addition to the basic models, models that cover thermal and irradiation (fast neutron flux) creep and swelling are also included.[120] Fuel cladding chemical interaction (FCCI) models, critically important for predicting cladding mechanical performance and failure, are also implemented.

While many of the empirical models from sources such as the Metallic Fuels Handbook[120] (MFH) are included in BISON, new models and updated parameters for existing models (Beeler et al.[124]) are being developed from lower-length-scale calculations. This approach provides fuel designers with material models beyond standard measurement-bound empirical models, gaining more insight into the underlying physics.

VI.B. Material and Behavior Models

The thermal conductivity model used in BISON for U, U-Zr, and U-Pu-Zr alloys is provided in the MFH (Ref. 120), which was developed from many sets of measurements compiled in Kittel et al.[125] This model is a function of zirconium and plutonium concentration and temperature. A model for specific heat is taken from Savage[126] and is a function of temperature and phase (where it is assumed that the phase simply changes with temperature). An average value for fuel thermal expansion, applicable in the temperature range of 293 to 1200 K, is taken from Saller et al.[127] The MFH (Ref. 120) is again used for elastic constants and creep models. The elastic constants are functions of temperature, porosity, and zirconium and plutonium concentration, whereas the models for steady-state thermal and irradiation creep depend on porosity, activation energy, effective stress, fission rate, and temperature. The solid and gaseous fission product swelling model comes from Olander,[128] the latter derived by a simple force balance of a bubble within a deformable solid and an equation of state for the gas behavior. The gaseous swelling model depends on temperature, bubble surface tension, fission rate and yield, time, and bubble number density. The relationship between porosity generation and gaseous swelling, also referenced in Olander, is used in BISON. The fission gas model is simply based on the fission rate for gas generation, and the fission gas released is governed by the value of porosity: When the porosity reaches 25%, 80% of the fission gas produced up to that point is released and all fission gas produced thereafter is immediately released.[129] Zirconium diffusion coefficients for U-Zr from Adda et al.[130] and Müller[131] at various temperatures are used in BISON. For more detail about how diffusion is modeled in BISON, see Galloway et al.[132]

Cladding material models consist of three variations of stainless steel: 316, D9, and HT9. Creep rate models for 316 are taken from the Nuclear Systems Materials Handbook[133] for the 20% cold-worked condition and Garner and Porter[134] for the annealed condition. The coefficient of thermal expansion for 316 is taken from the ASME Boiler and Pressure Vessel Code.[135] The thermal conductivity and heat capacity models for D9 are from Leibowitz and Blomquist[136] and Banerjee et al.,[137] respectively. The D9 models for thermal expansion, elastic moduli, creep rate, and swelling from the MFH are available in BISON. Finally, models for HT9 are taken from the MFH for thermal conductivity and creep rate, Leibowitz and Blomquist[136] for thermal expansion, Yamanouchi et al.[138] for heat capacity, and Los Alamos National Laboratory[139] for elastic moduli.

Accurately modeling the gap between fuel and cladding is important for representing heat transfer and FCCI. Heat transfer across the gap is modeled via BISON's thermal contact model, assuming constant thermal conductivity of the sodium and constant gap conductance. Due to the high thermal conductivity of the fuel and sodium, this is a valid assumption. There are several models for FCCI in BISON, consisting of work from Bauer et al.,[140] Karahan and Buongiorno,[141] Jiang et al.,[142] and Argonne National Laboratory's LIFE-METAL code.

VI.C. Assessment Case

The EBR-II X441 experiment was chosen as the initial case for BISON to model due to the number of fuel rod design parameters varied during the tests. Table II summarizes the variations in each group of fuel rods tested in the experiment. All of these groups were modeled using BISON and are part of the assessment cases included in the code repository.

Figure 5 shows the general features of an EBR–II fuel rod. The fuel is surrounded by a liquid sodium bond material in order to enhance the heat transfer between the fuel and the cladding. The remainder of the plenum volume is filled with He gas, as is typical in other fuel types (i.e., LWRs). The cladding material is generally a 316 stainless steel or similar stainless steel alloy.

The X441 "as-designed" geometry was used to create the BISON models, and a simplified power history and gap conductance were used in these simulations. In addition, the effects of Zr-redistribution and frictional contact were ignored in order to improve the robustness of the full set of X441 assessment cases. Figure 6 shows a comparison between EBR-II data and BISON predictions for the radial cladding strain as a function of the plenum-to-fuel volume ratio. The general trend in the data is for the radial strain to decrease as the plenum-to-fuel volume ratio increases. The BISON results show a similar trend, though not in complete agreement with the data. The BISON simulations should better match the data as the simplifications in the model are removed and more accurate power history and gap conductance inputs are used.

VI.D. Multiscale

As mentioned previously, progress has been made on using physics-based lower-length-scale calculations to inform engineering-scale calculations. One example is the development of a quantitative phase-field model of macroscale constituent redistribution in the U-Zr system, where model parameters were optimized and the model validated against an independent data set.[143] A second example is Beeler et al.'s calculation[124] of surface tension based on molecular dynamics, which is used in the BISON gaseous metallic fuel swelling model. Implementation of more lower-length-scale calculations to replace or inform existing empirical models is a central theme in future BISON development.

VII. CENTRAL VOID FORMATION IN MOX

An important feature of oxide fuel in fast reactors or LWRs at high temperature is central void formation. The coupled conservation equations necessary to represent this phenomenon are heat conduction and pore migration. To model pore migration, we assume pores are ubiquitous and uniformly distributed in the ceramic fuel. Upon heating, the pores undergo a complicated process of vaporizing on the hot side of the pore (nearer to the fuel centerline) and condensing on the cool side. The speed of this process is a highly uncertain quantity and has been the subject of considerable study.[128,144–150] Reference 151 describes how BISON is used to solve these equations. The following section includes a result from that paper concerning quantification of the effects of void offset.

TABLE II

X441 Experimental Parameters

Group	Plenum/ Fuel (Volume Ratio)	Zr Content (Weight Percent)	Smear Density (% Theoretical Density)	Clad Material	Clad Thickness (mils)
A	1.5	10	75	HT9	15
B	2.1	10	75	HT9	15
C	1.1	10	75	HT9	15
D	1.5	6	75	HT9	15
E	1.5	14	75	HT9	15
F	1.5	10	85	HT9	15
G	1.5	10	70	HT9	15
H	1.5	10	75	HT9	18

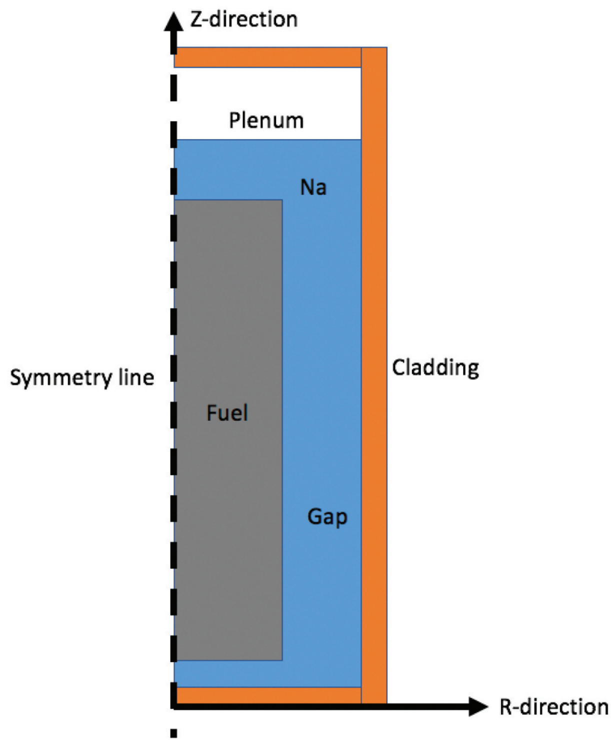

Fig. 5. Schematic illustration of a fuel rod for EBR-II (not to scale).

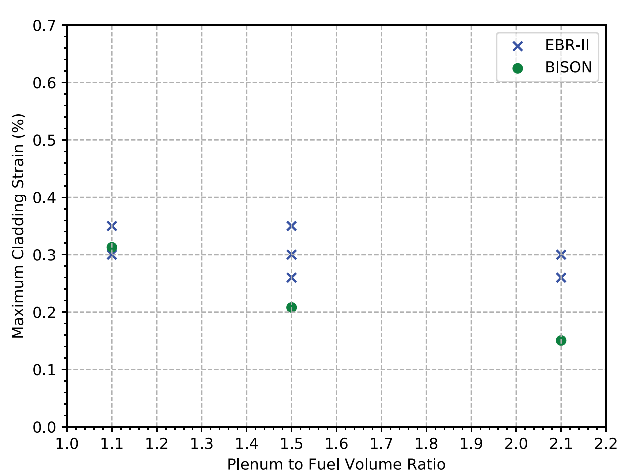

Fig. 6. Maximum cladding radial strain versus plenum-to-fuel volume ratio for the EBR-II X441 experiment.

VII.A. Multidimensional Effects

A 2-D calculation was run to demonstrate the effects of offset fuel within the cladding. The expectation was that an offset fuel pellet will get hotter on the side with the larger pellet/clad gap; consequently, the central void formation will also be offset. Results are shown in Figs. 7a and 7b when solving only pore migration and the heat equation (fuel and cladding displacements were neglected). A micrograph showing similar offset behavior is shown in Fig. 7c.

When comparing the calculations in Fig. 7b to the micrograph in Fig. 7c, measurements from a plot digitizer show than the calculation over predicts void offset by about 40%. We speculate this is due to neglecting mechanics (fuel expansion and cladding creep down). Refinements to this calculation are expected in a future publication.

VIII. VERIFICATION AND VALIDATION

A variety of processes have been developed to quantify the reliability and predictive capability of modeling and simulation tools.[153–155] These processes can be categorized into three main categories: (1) SQA is the process to detect unintentional coding mistakes in software (e.g., performing unit-, component-, and system-level defect analyses, regression tests, and code comparisons), (2) verification is the process to ensure that the code functions correctly (e.g., comparisons between code results and analytic or approximate analytic solutions), and (3) validation is the process of assessing a code's capability to accurately model physical problems (e.g., comparisons between code results and experiments). The applications of these procedures form the basis of code development in BISON, ensuring it is free of coding mistakes and that it accurately represents reality.[6,7,58,156,157] BISON SQA practices are outlined in Sec. II.C. Sections VIII.A and VIII.B briefly summarize BISON verification and validation activities.

VIII.A. Verification

A concise application of verification is to calculate the formal order of accuracy of a numerical discretization, followed by a test to see if the observed order matches. Code verification is performed by calculating the observed order of accuracy and comparing it to an analytically derived exact solution. In practice, exact solutions are difficult to obtain for systems that involve coupled differential equations. It is often necessary to calculate the observed order of accuracy by comparing the results from successive refinements of the solution domain, a process referred to as solution verification.

Here we provide two test problems for each verification method: (1) a spherical shell problem with an analytic solution (Fig. 8) and (2) an axisymmetric cylinder problem without an analytic solution (Fig. 9). Temperature results are shown for different meshes and finite elements in

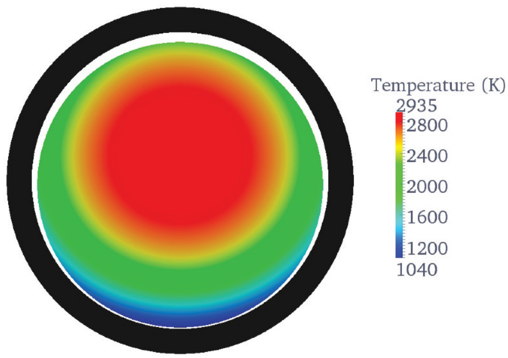

(a) Temperature (K), offset case.

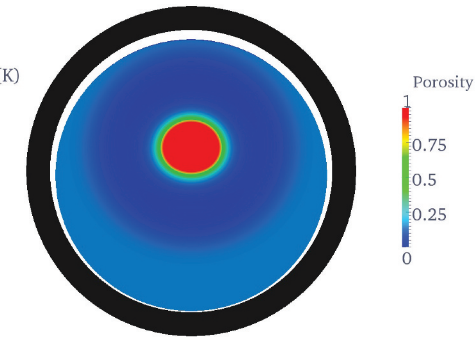

(b) Porosity, offset case.

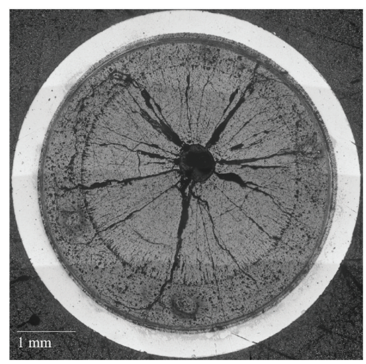

(c) Micrograph from Chichester [152].

Fig. 7. Two-dimensional calculation showing temperature and porosity contours in a restructured fuel pellet in offset (a and b) positions relative to the cladding. The offset and shape of this void is similar to the micrograph shown in (c), which is from a similar fuel pin subjected to conditions consistent with the model shown in (a) and (b). Measurement using a plot digitizer on the images show that the calculation over predicts void offset by about 40%.

which BISON accurately predicts the temperature distribution. Then a convergence study is conducted with a refinement factor of two (i.e., $r = 2$). The error behavior is compared to the expected behavior to quantify the success of each problem as the mesh is refined. The error norm is computed as $||y - \tilde{y}|| = Ch^{p+1}$ in terms of the expected solution to a problem y, the numerical approximation $\tilde{y}$, the order of accuracy p, the mesh spacing h, and an arbitrary constant C. The computed norms for each element type are plotted. The observed order of accuracy is obtained from the slope of the error norm in a log-log plot (i.e., $p + 1 = \log(||y - \tilde{y}||)/\log(h)$ in the asymptotic

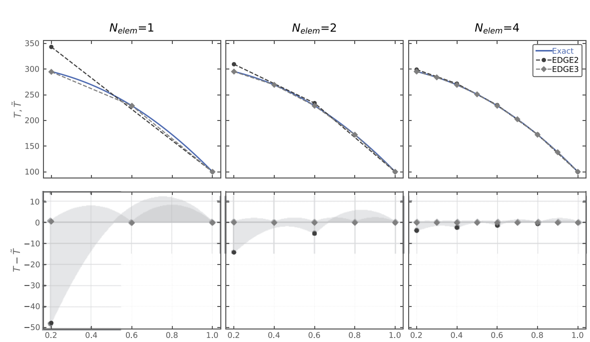

(a) Temperature distributions (first row) and residual (second row) for different meshes and finite elements.

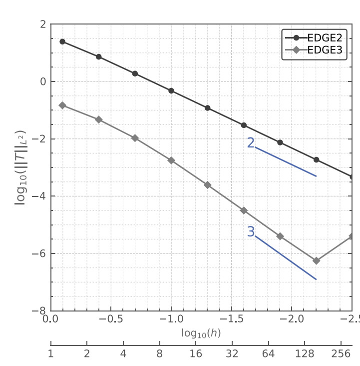

(b) Convergence plot ($r_r = 2$).

Fig. 8. Code verification: BISON results are computed using 1-D finite elements (shape: line, EDGE2: linear, EDGE3: quadratic) for a spherical shell that is exposed on its outer surface to a constant temperature and has a constant heat flux applied to its inner surface. The shell has isotropic material properties and uniform internal heating.[156,158]

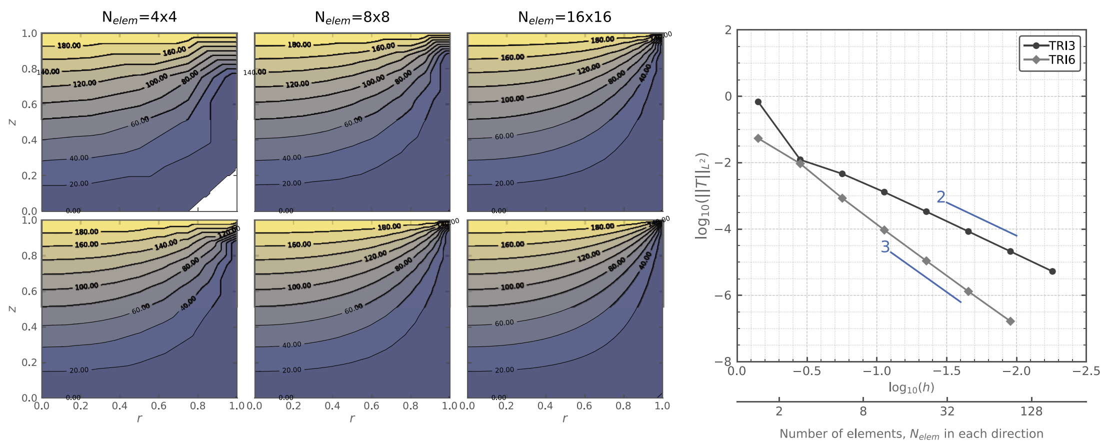

(a) Temperature distribution for different meshes and finite elements (first row: TRI3, second row: TRI6).

(b) Convergence plot ($r_r = r_z = 2$).

Fig. 9. Solution verification: BISON results are computed using 2-D finite elements (shape: triangular, TRI3: linear, TRI6: quadratic) for an axisymmetric cylinder exposed on its bottom and right surfaces to a constant temperature of T_1 (=0 K in this study) and on its top surface to a constant temperature of T_2 (=200 K in this study). The cylinder has isotropic material properties with no internal heating.[156]

region). The formal order of accuracy, theoretically derived in Refs. 156 and 157, is shown (labeled 2 and 3) in Figs. 8 and 9. Note that the finite element orders are $p = 1$ and 2 for linear and quadratic polynomials, respectively. The elements each show the correct order of convergence. These results indicate that, at least for the code exercised in the examples, BISON functions as intended and is free of coding mistakes.

A thorough pedigree of verification in BISON is established in Refs. 6, 156, and 157 by performing an extensive verification study and creating verification matrices that cover conservation terms, geometry, and discretization choices.

VIII.B. Validation

After the quality assurance of the code and verification of its numerics, it is essential to validate that the code is capable of accurately modeling the actual behavior of real-world problems by comparing its predictions to experimental data. Two types of validation tests are performed in BISON to address this: (1) Separate-effects validation tests investigate a code's capability to model a single physical phenomenon such as hydrogen migration and distribution in the zirconium-based nuclear fuel cladding,[159] and (2) integral-effects validation tests examine a system's overall response to a model that involves many phenomena. BISON has undergone substantial validation over the years regarding its modeling capability for nuclear fuel rod behavior under normal operating conditions and design-basis accident scenarios. Table III briefly summarizes BISON's validation activities for the aforementioned nuclear fuel types. All validation activities have been analyzed, documented, and incorporated into BISON's validation suite.

IX. CURRENT AND FUTURE DIRECTIONS

BISON's capabilities continue to grow in each of the areas reviewed in this paper. Modeling of traditional LWR fuel rods is being enhanced through improved support of lower-dimensional analysis. The so-called 1.5-D or layered approach to modeling a fuel rod involves representing the rod as stacked slices, with each slice an axisymmetric, 1-D representation of a section of the rod. This technique is being expanded to a 2.5-D capability where each slice is a 2-D cross section of the rod. This new capability will combine efficient calculation with the ability to model azimuthally varying conditions. Other work in this area includes continued research into fission gas behavior and a continual effort to add more validation cases, particularly LOCA and RIA cases.

While improving models for ATF continues, considerable effort is now being made to improve modeling at high-burnup conditions. Running fuel rods to high burnup, combined with increased initial enrichment, is economically advantageous. However, fuel rod behavior at high burnup, particularly accident behavior, requires more development. Understanding fuel and cladding interactions and fuel fragmentation at high burnup is essential to this effort. The BISON team is partnering with others at INL, as well as researchers outside INL, to improve our modeling capabilities in this area.

TABLE III

Validation Matrix for BISON Fuel Behavior

			Configurations				Measurements			
Experiment	Reference	Cases	Final Burnup (MWd/kgU)	Fuel Material	Cladding Material	Coolant Pressure Temperature	Temperature	FGR	Dimension[a]	Energy
LWR fuel rod behavior (under normal operating conditions)										
IFA-431 rods 1, 2, 3, 4 (3-D)	160 and 162	4	≈4	UO_2	Zr-2		✓			
IFA-432 rods 1, 2, 3	160, 162, and 163	3	≈32	UO_2	Zr-2		✓			
IFA-515.10 rod A1	164	1	≈76	UO_2	Zr-2		✓			
IFA 519 rods DH, DK	165	2	≈90	UO_2	Zr-4			✓		
IFA-534 rods 18, 19	166, 167 and 168	2	52 to 55	UO_2	Zr-4			✓	✓	
IFA-535.5-6 rods 809, 810, 811, 812	169 and 170	4	44	UO_2	Zr-2		✓	✓	✓	
IFA-562.2 rods 15, 16, 17	171	3	≈50	UO_2	Zr-2		✓			
IFA-597.3 rods 7, 8	166, 172, and 173	1		UO_2	Zr-2		✓	✓	✓	
IFA-636.2 rod 5	174	1		UO_2	Zr-4				✓	
IFA-677.1 rod 1	175, 176, and 177	1	≈26.3	UO_2	Zr-4		✓	✓	✓	
Risø-2 GE-m	169 and 178	1	14	UO_2	Zr-2			✓	✓	
Risø-3 AN2–4, AN8	166, and 179 through 182	7	41 to 44	UO_2	Zr-4		✓	✓	✓	
Risø-3 GE7, II3, II5	166, 183, and 184	7		UO_2	Zr-2		✓	✓	✓	
OSIRIS H09, J12-5	169 and 185	2	24 to 46	UO_2	Zr-2/4			✓	✓	
REGATE	166	1	47	UO_2·	Zr-2			✓	✓	
USPWR(16 × 16) TSQ002, TSQ022	169	2	≈58	UO_2	Zr-4		✓	✓	✓	
R.E. Ginna Rodlet-2, Rodlet-4	186	2	51 to 57	UO_2	Zr-4			✓	✓	
High Burnup Effects Programme A1/8-4, A3/6-4, H8/36-4	187	3	47 to 49	UO_2	Zr-2			✓	✓	
High Burnup Effects Programme BK363, BK365, BK370	166 and 187	3	51 to 69	UO_2	Zr-4			✓		
Tribulation BN1/3, BN1/4, BN3/15	188	3	≈51	UO_2	Zr-4			✓	✓	

(Continued)

TABLE III (Continued)

			Configurations				Measurements			
Experiment	Reference	Cases	Final Burnup (MWd/kgU)	Fuel Material	Cladding Material	Coolant Pressure Temperature	Temperature	FGR	Dimension[a]	Energy
LWR fuel rod behavior (under LOCA conditions)										
REBEKA	62, 75, and 189	20		UO_2	Zr-4	H_2O, 1 to 14 MPa, 573 to 1310 K	✓			
PUZRY	190, 191, and 192	31		UO_2	Zr-4	Ar, 0.5 to 10 MPa, 973 to 1473 K			✓	
Hardy	193	15		UO_2	Zr-4	Vacuum, 0.3 to 14 MPa, 600 to 1600 K	✓			
ORNL	194	3		UO_2	Zr-2/4	He, 6 to 9 MPa, 380 to 1100 K	✓			
QUENCH-L1	195	2		UO_2	Zr-4	H_2O-Ar, 5.5 to 6 MPa, 300 to 1470 K	✓	✓	✓	
IFA-650.2, .9, .10	196, 197, and 198	3	0–90	UO_2	Zr-4		✓		✓	
LWR fuel rod behavior (under RIA conditions)										
CABRI REP Na.2, 3, 4, 5, 10 (17 × 17)	199, 200, and 201	5		UO_2	Zr-4	Na, 0.5 MPa, 553 K		✓	✓	✓
CABRI CIP0-1 (17 × 17)	199, 200, and 201	1		UO_2	ZIRLO	Na, 0.5 MPa, 553 K				
CABRI CIP3-1 (17 × 17)	199, 200, and 201	1		UO_2	ZIRLO	H_2O, 16 MPa, 280 K				

ATF rod behavior										
ATR ATF R4, R6 IFA-677.1 rods 1, 5	87 176, 177, and 202	2 2	17–20 ~ 26	U_3Si_2 Cr_2O_3-Doped UO_2	ZIRLO Zr-4		 ✓	✓ ✓	✓ ✓	
IFA-716.1 rods 1	203, 204, and 205	1	~ 27	Cr_2O_3-Doped UO_2	Zr-4		✓	✓	✓	
TRISO fuel behavior										
IAEA Coordinated Research Program 6 (benchmark)	206	13		UO_2	PyC/SiC		✓	✓	✓	
Metallic fuel rod behavior										
EBR II X441 TREAT M7	 207	8 1		U–Pu–Zr U–Zr	HT9 HT9		 ✓		✓ 	
MOX fuel rod behavior										
FFTF FO 2 fuel pin L 09	208	1		MOX	HT9	Na, 0.151 MPa, 580 K		✓	✓	
JOYO B14	209	4		MAMOX	HT9		✓		✓	

[a]Dimensional changes (e.g., displacements, corrosion thickness, central void formation, etc.) or rod internal pressure.

Modeling of TRISO fuel is seeing much greater interest, with advanced reactor developers, microreactor developers, and developers of nuclear thermal propulsion for space applications all expressing interest. Current work in TRISO modeling includes improved sampling and statistical capabilities, research into fission product diffusion, and validation to experimental data.

Metallic fuel modeling research in BISON is focused on fuel swelling. Fuel swelling in metallic fuels is complicated by its anisotropic nature and its coupling to fission gas behavior. Other work on metallic fuel modeling includes the redistribution of zirconium during irradiation.

In each of these areas, improved verification testing and validation are major efforts.

BISON is intended to be a true multifuel code, providing a full range of capabilities for each major nuclear fuel type while allowing users to customize behavior through the addition of new material or behavioral models. BISON includes documentation for each of its capabilities that is packaged directly with the source code. The developmental process follows NQA-1 guidelines and relies on extensive integration testing and code reviews to ensure high quality. Verification and validation cases are run regularly and are included with the code, allowing users to evaluate the adequacy of BISON for their purposes. BISON is a platform for research in nuclear fuel performance modeling while simultaneously serving as a tool for the analysis of nuclear fuel designs. The flexibility of BISON makes it unique among nuclear fuel performance applications.

Acknowledgments

This work was funded by DOE under the Nuclear Energy Advanced Modeling and Simulation and the Consortium for the Advanced Simulation of Light Water Reactors programs. The submitted manuscript has been authored by a contractor of the U.S. government under contract DE-AC07-05ID14517. Accordingly, the U.S. government retains a nonexclusive, royalty-free license to publish or reproduce the published form of this contribution, or allow others to do so, for U.S. government purposes.

ORCID

Jason D. Hales http://orcid.org/0000-0003-0836-0476
Aysenur Toptan http://orcid.org/0000-0003-4250-6336
Christoper Matthews http://orcid.org/0000-0003-1468-1348

References

1. P. VAN UFFELEN et al., "A Review of Fuel Performance Modeling," *J. Nucl. Mater.*, **516**, 373 (2019); https://doi.org/10.1016/j.jnucmat.2018.12.037.

2. R. L. WILLIAMSON et al., "Multidimensional Multiphysics Simulation of Nuclear Fuel Behavior," *J. Nucl. Mater.*, **423**, *1–3*, 149 (2012); https://doi.org/10.1016/j.jnucmat.2012.01.012.

3. C. J. PERMANN et al., "MOOSE: Enabling Massively Parallel Multiphysics Simulation," *SoftwareX*, **11**, 100430 (2020); https://doi.org/10.1016/j.softx.2020.100430.

4. R. L. WILLIAMSON, "Enhancing the ABAQUS Thermomechanics Code to Simulate Multipellet Steady and Transient LWR Fuel Rod Behavior," *J. Nucl. Mater.*, **415**, *1*, 74 (2011); https://doi.org/10.1016/j.jnucmat.2011.05.044.

5. J. D. HALES et al., "Multidimensional Multiphysics Simulation of TRISO Particle Fuel," *J. Nucl. Mater.*, **443**, *1–3*, 531 (2013); https://doi.org/10.1016/j.jnucmat.2013.07.070.

6. J. HALES et al., "Verification of the BISON Fuel Performance Code," *Ann. Nucl. Energy*, **71**, 81 (2014); https://doi.org/10.1016/j.anucene.2014.03.027.

7. R. WILLIAMSON et al., "Validating the BISON Fuel Performance Code to Integral LWR Experiments," *Nucl. Eng. Des.*, **301**, 232 (2016); https://doi.org/10.1016/j.nucengdes.2016.02.020.

8. S. NOVASCONE et al., "Evaluation of Coupling Approaches for Thermomechanical Simulations," *Nucl. Eng. Des.*, **295**, 910 (2015); https://doi.org/10.1016/j.nucengdes.2015.07.005.

9. M. R. TONKS et al., "Mechanistic Materials Modeling for Nuclear Fuel Performance," *Ann. Nucl. Energy*, **105**, 11 (2017); https://doi.org/10.1016/j.anucene.2017.03.005.

10. S. R. NOVASCONE et al., "Summary of BISON Milestones and Activities—NEAMS FY19 Report," INL/EXT-19-55699, Idaho National Laboratory (2019).

11. L. AAGESEN et al., "Marmot Modeling of Swelling in U-Zr and Integration into BISON," INL/EXT-19-55959, Idaho National Laboratory (2019).

12. G. KHVOSTOV, W. LYON, and M. ZIMMERMANN, "Application of the FALCON Code to PCI Induced Cladding Failure and the Effects of Missing

Pellet Surface," *Ann. Nucl. Energy*, **62**, 398 (2013); https://doi.org/10.1016/j.anucene.2013.07.002.

13. Y. ALESHIN et al., "The Effect of Pellet and Local Power Variations on PCI Margin," *Proc. Top Fuel 2010*, Orlando, Florida, September 26–29, 2010.
14. J. LEE et al., "The Mechanical Behavior of Pellet-Cladding with the Missing Chip Under PCMI Loadings During Power Ramp," *Proc. 2007 LWR Fuel Performance Mtg./TopFuel 2007 "Zero by 2010,"* San Francisco, California, September 30–October 3, 2007.
15. B. SPENCER et al., "3D Modeling of Missing Pellet Surface Defects in BWR Fuel," *Nucl. Eng. Des.*, **307**, 155 (2016); https://doi.org/10.1016/j.nucengdes.2016.07.008.
16. R. L. WILLIAMSON et al., "Summary of BISON Development and Validation Activities—NEAMS FY16 Report," INL/EXT-16-40071, Idaho National Laboratory (2016).
17. J. D. HALES et al., "1.5D BISON Simulation Capability," INL/EXT-16-40785, Idaho National Laboratory (2017).
18. K. A. GAMBLE, "Axial Relocation Model Extension in Bison," CASL-U-2018-1662-000 Rev.1, Idaho National Laboratory (2018).
19. S. A. PITTS et al., "Verify and Validate 1.5D Capability," CASL-U-2017-1380 Rev.1, Idaho National Laboratory (2018).
20. T. DOWNAR et al., "MPACT Theory Manual, Version 2.2.0," ORNL/TM-2016/476, Oak Ridge National Laboratory (2016); https://doi.org/10.2172/1340449.
21. R. SALKO Jr et al., "CTF 4.0 Theory Manual," ORNL/TM-2019/1145, Oak Ridge National Laboratory (2019); https://doi.org/10.2172/1550750.
22. S. STIMPSON et al., "Coupled Fuel Performance Calculations in VERA and Demonstration on Watts Bar Unit 1, Cycle 1," *Ann. Nucl. Energy*, **145**, 107554 (2020); https://doi.org/10.1016/j.anucene.2020.107554.
23. R. L. WILLIAMSON et al., "LOCA Challenge Problem Final Report," CASL-U-2019-1856-000, Consortium for Advanced Simulation of Light Water Reactors (2019).
24. R. GARDNER et al., "Demonstration of BISON-TRACE Coupling (CRAB) Through Validation Case LOFT L2-5," *Proc. TopFuel 2019*, Seattle, Washington, September 22–26, 2019.
25. S. A. PITTS et al., "Bison Documentation Expansion for Tensor Mechanics and Layered1D Capabilities," INL/EXT-18-45780, Idaho National Laboratory (2018).
26. R. L. WILLIAMSON et al., "BISON Manual," INL-MIS-18-50577-Rev3, Idaho National Laboratory (2020).
27. A. SLAUGHTER et al., "NEAMS-IPL MOOSE Midyear Framework Activities," INL/EXT-18-45020, Idaho National Laboratory (2018).
28. A. E. SLAUGHTER et al., "Continuous Integration, In-Code Documentation, and Automation for Nuclear Quality Assurance Conformance," *Nucl. Technol.*, **207**, 923 (2021); https://doi.org/10.1080/00295450.2020.1826804.
29. "BISON Code Documentation," Idaho National Laboratory (July 2020); https://mooseframework.org/bison/syntax/bison_only_index.html.
30. "Software Quality Assurance Plan for MOOSE and MOOSE-Based Applications," Document ID: PLN-4005, Rev. 7, Idaho National Laboratory (2020).
31. G. PASTORE et al., "Modelling of Fuel Behaviour During Loss-of-Coolant Accidents Using the BISON Code," *Proc. LWR Fuel Performance Mtg.*, Zurich, Switzerland, September 13 –17, 2015 (2015).
32. R. L. WILLIAMSON et al., "Reactivity Insertion Accident (RIA) Capability Status in the BISON Fuel Performance Code," CASL-X-2016-1104-000, Oak Ridge National Laboratory (2016).
33. G. PASTORE et al., "Modelling Fission Gas Behaviour with the BISON Fuel Performance Code," presented at the Enlarged Halden Programme Group Mtg., Lillehammer, Norway, September 24 –29, 2017.
34. C. P. FOLSOM et al., "Development of a RIA Experimental Benchmark for BISON," CASL-U-2017-1403-000, Oak Ridge National Laboratory (2017).
35. G. PASTORE et al., "Analysis of Fuel Rod Behavior During Loss-of-Coolant Accidents Using the BISON Code: Cladding Modeling Developments and Simulation of Separate-effects Experiments," *J. Nucl. Mater.*, 152537 (2020); https://doi.org/10.1016/j.jnucmat.2020.152537.
36. G. PASTORE et al., "Analysis of Fuel Rod Behavior During Loss-of-Coolant Accidents Using the BISON Code: Fuel Modeling Developments and Simulation of Integral Experiments," *J. Nucl. Mater*, **545**, 152645 (2020); https://doi.org/10.1016/j.jnucmat.2020.152645.
37. A. MARION (NEI) letter dated June 13, 2006 to H. N. Berkow (U.S. NRC/NRR), "Safety Evaluation by the Office of Nuclear Reactor Regulation of Electric Power Research Institute (EPRI) Topical Report TR-1002865," and "Topical Report on Reactivity Initiated Accidents: Bases for RIA Fuel Rod Failures and Core Coolability Criteria" (2006); http://pbadupws.nrc.gov/docs/ML0616/ML061650107.pdf (current as of July 10, 2020).
38. A. SOBA et al., "A High Burnup Model Developed for the DIONISIO Code," *J. Nucl. Mater.*, **433**, *1–3*, 160 (2013); https://doi.org/10.1016/j.jnucmat.2012.08.016.
39. A. SOBA et al., "Simulation of the Behaviour of Nuclear Fuel Under High Burnup Conditions," *Ann. Nucl. Energy*, **70**, 147 (2014); https://doi.org/10.1016/j.anucene.2014.03.004.

40. Y. R. RASHID, "Mathematical Modeling and Analysis of Fuel Rods," *Nucl. Eng. Des.*, **29**, *1*, 22 (1974); https://doi.org/10.1016/0029-5493(74)90095-8.

41. T. BARANI et al., "Isotropic Softening Model for Fuel Cracking in BISON," *Nucl. Eng. Des.*, **342**, 257 (2019); https://doi.org/10.1016/j.nucengdes.2018.12.005.

42. S. C. MANUAL, "Volume 4: MATPRO A Library of Materials Properties for Light-Water-Reactor Accident Analysis," INEEL/EXT-02-00589, Idaho National Engineering and Environmental Laboratory (2003).

43. Y. RASHID, R. DUNHAM, and R. MONTGOMERY, "Fuel Analysis and Licensing Code: FALCON MOD01," EPRI 1011308, Electric Power Research Institute (2004).

44. G. PASTORE et al., "Physics-Based Modelling of Fission Gas Swelling and Release in UO_2 applied to Integral Fuel Rod Analysis," *Nucl. Eng. Des.*, **256**, 75 (2013); https://doi.org/10.1016/j.nucengdes.2012.12.002.

45. G. PASTORE et al., "Uncertainty and Sensitivity Analysis of Fission Gas Behavior in Engineering-Scale Fuel Modeling," *J. Nucl. Mater.*, **456**, 398 (2015); https://doi.org/10.1016/j.jnucmat.2014.09.077.

46. J. B. AINSCOUGH, B. W. OLDFIELD, and J. O. WARE, "Isothermal Grain Growth Kinetics in Sintered UO_2 Pellets," *J. Nucl. Mater.*, **49**, *2*, 117 (1973); https://doi.org/10.1016/0022-3115(73)90001-9.

47. E. M. A. KRAMMAN and H. R. FREEBURN, "ESCORE —The EPRI Steady-State Core Reload Evaluator Code: General Description," EPRI NP-5100, Electric Power Research Institute (1987).

48. L. P. SWILER, R. L. WILLIAMSON, and D. M. PEREZ, "Calibration of a Fuel Relocation Model in BISON," *Proc. Int. Conf. on Mathematics and Computational Methods Applied to Nuclear Science and Engineering*, Sun Valley, Idaho, May 5–9, 2013.

49. M. LIMBÄCK and T. ANDERSSON, "A Model for Analysis of the Effect of Final Annealing on the In- and Out-of-Reactor Creep Behavior of Zircaloy Cladding," *Zirconium in the Nuclear Industry: 11th Int. Symp.*, ASTM STP 1295, West Conshohocken, Pennsylvania, 448 (1996).

50. D. G. FRANKLIN, "Zircaloy-4 Cladding Deformation During Power Reactor Irradiation," *Proc. Zirconium in the Nuclear Industry: 15th Int. Symp.*, D. G. FRANKLIN, Ed., 235, ASTM STP 754, West Conshohocken, Pennsylvania (1982).

51. M. HEINSTEIN and T. LAURSEN, "An Algorithm for the Matrix-Free Solution of Quasistatic Frictional Contact Problems," *Int. J. Numer. Methods Eng.*, **44**, *9*, 1205 (1999); https://doi.org/10.1002/(SICI)1097-0207(19990330)44:9<1205::AID-NME550>3.0.CO;2-0.

52. A. M. ROSS and R. L. STOUTE, "Heat Transfer Coefficient Between UO_2 and Zircaloy-2," AECL-1552, Atomic Energy of Canada Limited (1962).

53. D. D. LANNING and C. R. HANN, "Review of Methods Applicable to the Calculation of Gap Conductance in Zircaloy-Clad UO_2 Fuel Rods," BWNL-1894, UC-78B, Pacific Northwest National Laboratory (1975).

54. C. M. ALLISON et al., "SCDAP/RELAP5/MOD3.1 Code Manual, Volume IV: MATPRO–A Library of Materials Properties for Light-Water-Reactor Accident Analysis," NUREG/CR-6150, EGG-2720, Idaho National Engineering Laboratory (1993).

55. A. TOPTAN, D. KROPACZEK, and M. AVRAMOVA, "On the Validity of the Dilute Gas Assumption for Gap Conductance Calculations in Nuclear Fuel Performance Codes," *Nucl. Eng. Des.*, **350**, 1 (2019); https://doi.org/10.1016/j.nucengdes.2019.04.042.

56. A. TOPTAN, D. KROPACZEK, and M. AVRAMOVA, "Gap Conductance Modeling I: Theoretical Considerations for Single- and Multi-Component Gases in Curvilinear Coordinates," *Nucl. Eng. Des.*, **353**, 110283 (2019); https://doi.org/10.1016/j.nucengdes.2019.110283.

57. A. TOPTAN, D. KROPACZEK, and M. AVRAMOVA, "Gap Conductance Modeling II: Optimized Model for UO_2 -Zircaloy Interfaces," *Nucl. Eng. Des.*, **355**, 110289 (2019); https://doi.org/10.1016/j.nucengdes.2019.110289.

58. A. TOPTAN et al., "Modeling of Gap Conductance for LWR Fuel Rods Applied in the BISON Code," *J. Nucl. Sci. Technol.*, **57**, *8*, 963 (2020); https://doi.org/10.1080/00223131.2020.1740808.

59. L. O. JERNKVIST and A. MASSIH, "Model for Axial Relocation of Fragmented and Pulverized Fuel Pellets in Distending Fuel Rods and Its Effects on Fuel Rod Heat Load," SSM-2015:37, Strål säkerhets myndigheten (2015).

60. G. SCHANZ, "Recommendations and Supporting Information on the Choice of Zirconium Oxidation Models in Severe Accident Codes," FZKA 6827, SAM-COLOSS-P043, Forschungszentrum Karlsruhe (2003).

61. A. MASSIH, "Transformation Kinetics of Zirconium Alloys Under Non-Isothermal Conditions," *J. Nucl. Mater.*, **384**, *3*, 330 (2009); https://doi.org/10.1016/j.jnucmat.2008.11.033.

62. F. J. ERBACHER et al., "Burst Criterion of Zircaloy Fuel Claddings in a Loss-of-Coolant Accident," *Zirconium in the Nuclear* Industry, *5th Conf.*, ASTM STP 754, D.G. FRANKLIN, Ed., 271, West Conshohocken, Pennsylvania (1982).

63. V. DI MARCELLO et al., "The TRANSURANUS Mechanical Model for Large Strain Analysis," *Nucl. Eng. Des.*, **276**, 19 (2014); https://doi.org/10.1016/j.nucengdes.2014.04.041.

64. K. GEELHOOD, C. BEYER, and W. LUSCHER, "PNNL Stress/Strain Correlation for Zircaloy," PNNL-17700, Pacific Northwest National Laboratory (2008).

65. G. PASTORE et al., "Modelling of Transient Fission Gas Behaviour in Oxide Fuel and Application to the BISON Code," presented at the Enlarged Halden Programme Group Mtg., Røros, Norway, September 7–12, 2014.

66. T. BARANI et al., "Analysis of Transient Fission Gas Behaviour in Oxide Fuel Using BISON and TRANSURANUS," *J. Nucl. Mater.*, **486**, 96 (2017); https://doi.org/10.1016/j.jnucmat.2016.10.051.

67. W. LIU et al., "BISON Application to the Analysis of LWR Fuel Responses Under Accident Conditions," *Proc. of TopFuel 2019*, Seattle, Washington, September 22–26, 2019.

68. N. CAPPS et al., "Evaluation of Missing Pellet Surface Geometry on Cladding Stress Distribution and Magnitude," *Nucl. Eng. Des.*, **305**, 51 (2016); https://doi.org/10.1016/j.nucengdes.2016.04.039.

69. N. CAPPS et al., "PCI Analysis of a Commercial PWR Using BISON Fuel Performance Code," *Nucl. Eng. Des.*, **324**, 131 (2017); https://doi.org/10.1016/j.nucengdes.2017.09.004.

70. S. STIMPSON et al., "Pellet-Clad Mechanical Interaction Screening Using VERA Applied to Watts Bar Unit 1, Cycles 1 –3," *Nucl. Eng. Des.*, **327**, 172 (2018); https://doi.org/10.1016/j.nucengdes.2017.12.015.

71. N. CAPPS et al., "Assessment of the Analysis Capability for Core-Wide PWR Pellet-Clad Interaction Screening of Watts Bar Unit 1," *Nucl. Eng. Des.*, **333**, 131 (2018); https://doi.org/10.1016/j.nucengdes.2018.04.018.

72. "Fuel Modelling at Extended Burnup (FUMEX-II)," IAEA-TECDOC-1687, International Atomic Energy Agency (2012).

73. "Improvement of Computer Codes Used for Fuel Behaviour Simulations (FUMEX-III)," IAEA-TECDOC -1697, International Atomic Energy Agency (2013).

74. "Fuel Modelling in Accident Conditions (FUMAC): Final Report of a Coordinated Research Project," IAEA-TECDOC-1889, International Atomic Energy Agency (2019).

75. F. ERBACHER, H. NEITZEL, and K. WIEHR, "Cladding Deformation and Emergency Core Cooling of a Pressurized Water Reactor in a LOCA. Summary Description of the REBEKA Program," KfK 4781, Kernforschungszentrum Karlsruhe (1990).

76. W. JIANG, B. W. SPENCER, and J. E. DOLBOW, "Ceramic Nuclear Fuel Fracture Modeling with the Extended Finite Element Method," *Eng. Fract. Mech.*, **223**, 106713 (2020); https://doi.org/10.1016/j.engfracmech.2019.106713.

77. Y. HU et al., "Thermomechanical Peridynamic Analysis with Irregular Non-Uniform Domain Discretization," *Eng. Fract. Mech.*, **197**, 92 (2018); https://doi.org/10.1016/j.engfracmech.2018.02.006.

78. S. BRAGG-SITTON et al., "Advanced Fuels Campaign Light Water Reactor Accident Tolerant Fuel Performance Metrics," INL/EXT-13-29957, Idaho National Laboratory (2014).

79. K. A. GAMBLE et al., "Nuclear Energy Advanced Modeling and Simulation (NEAMS) Accident Tolerant Fuels High Impact Problem: Engineering Scale Models and Analysis," INL/EXT-17-43388 Rev. 0, Idaho National Laboratory (2017).

80. K. A. GAMBLE, "ATF Material Model Development and Validation for Priority Cladding Concepts," CASL-U-2019-1892-000 Rev. 0, Idaho National Laboratory (2019).

81. K. A. GAMBLE et al., "ATF Material Model Development and Validation for Priority Fuel Concepts," CASL-U-2019-1870-000 Rev. 0, Idaho National Laboratory (2019).

82. Y. MIAO et al., "Gaseous Swelling of U_3Si_2 during Steady-State LWR Operation: A Rate Theory Investigation," *Nucl. Eng. Des.*, **322**, 336 (2017); https://doi.org/10.1016/j.nucengdes.2017.07.008.

83. T. BARANI et al., "Multiscale Modeling of Fission Gas Behavior in U_3Si_2 Under LWR Conditions," *J. Nucl. Mater.*, **522**, 97 (2019); https://doi.org/10.1016/j.jnucmat.2019.04.037.

84. J. T. WHITE, "Update to the U_3Si_2 Property Handbook," LA-UR-18-28719, Los Alamos National Laboratory (2018).

85. R. A. FREEMAN et al., "Analysis of Thermal Creep for Uranium Silicide Fuel Using Bison," *Proc. 2018 Int. Congress on Advances in Nuclear Power* Plants *(ICAPP 18*), Charlotte, North Carolina, April 8–11, 2018.

86. G. L. HOFMAN and W. S. RYU, "Detailed Analysis of Uranium Silicide Dispersion Fuel Swelling," CONF-8909141–10, Argonne National Laboratory (1989).

87. F. CAPPIA and J. M. HARP, "Postirradiation Examination of Low Burnup U_3Si_2 Fuel for Light Water Reactor Applications," *J. Nucl. Mater.*, **518**, 61 (2019); https://doi.org/10.1016/j.jnucmat.2019.02.047.

88. W. LI and K. SHIRVAN, "U_3Si_2-SiC Fuel Performance Analysis in BISON During Normal Operation," *Ann. Nucl. Energy*, **132**, 34 (2019); https://doi.org/10.1016/j.anucene.2019.04.021.

89. Y. HE et al., "Fuel Performance Optimization of U_3Si_2-SiC Design During Normal, Power Ramp and RIA Conditions," *Nucl. Eng. Des.*, **353**, 110276 (2019); https://doi.org/10.1016/j.nucengdes.2019.110276.

90. R. SWEET et al., "Performance of U_3Si_2 in an LWR Following a Cladding Breach During Normal Operation," *J. Nucl. Mater.*, **539**, 152263 (2020); https://doi.org/10.1016/j.jnucmat.2020.152263.
91. Y. CHE et al., "Modeling of Cr_2O_3 Doped UO_2 as a Near-Term Accident Tolerant Fuel for LWRs Using the BISON Code," *Nucl. Eng. Des.*, **337**, 271 (2018); https://doi.org/10.1016/j.nucengdes.2018.07.015.
92. K. TERRANI et al., "Uniform Corrosion of FeCrAl Alloys in LWR Coolant Environments," *J. Nucl. Mater.*, **479**, 36 (2016); https://doi.org/10.1016/j.jnucmat.2016.06.047.
93. Z. T. THOMPSON, K. A. TERRANI, and Y. YAMAMOTO, "Elastic Modulus Measurement of ORNL ATF FeCrAl Alloys," ORNL/TM-2015/632, Oak Ridge National Laboratory (2015).
94. N. M. GEORGE et al., "Neutronic Analysis of Candidate Accident-Tolerant Cladding Concepts in Pressurized Water Reactors," *Ann. Nucl. Energy*, **75**, 703 (2015); https://doi.org/10.1016/j.anucene.2014.09.005.
95. R. E. STACHOWSKI et al., "Progress of GE Development of Accident Tolerant Fuel FeCrAl Cladding," *Proc. of TopFuel 2016*, Boise, Idaho, September 11–15, 2016.
96. X. HU et al., "Hydrogen Permeation in FeCrAl Alloys for LWR Cladding Application," *J. Nucl. Mater.*, **461**, 282 (2015); https://doi.org/10.1016/j.jnucmat.2015.02.040.
97. K. A. GAMBLE et al., "An Investigation of FeCrAl Cladding Behavior Under Normal Operating and Loss of Coolant Conditions," *J. Nucl. Mater.*, **491**, 55 (2017); https://doi.org/10.1016/j.jnucmat.2017.04.039.
98. K. A. TERRANI, T. M. KARLSEN, and Y. YAMAMOTO, "Input Correlations for Irradiation Creep of FeCrAl and SiC Based on In-Pile Halden Test Results," ORNL/TM-2016/191, Oak Ridge National Laboratory (2016).
99. K. G. FIELD et al., "Handbook on the Material Properties of FeCrAl Alloys for Nuclear Power Production Applications," ORNL/SPR-2018/905 Rev. 1, Oak Ridge National Laboratory (2018).
100. X. WU, T. KOZLOWSKI, and J. D. HALES, "Neutronics and Fuel Performance Evaluation of Accident Tolerant FeCrAl Cladding Under Normal Operation Conditions," *Ann. Nucl. Energy*, **85**, 763 (2015); https://doi.org/10.1016/j.anucene.2015.06.032.
101. J. GALLOWAY and C. UNAL, "Accident-Tolerant-Fuel Performance Analysis of APMT Steel Clad/UO_2 Fuel," *Nucl. Sci. Eng.*, **182**, *4*, 523 (2016); https://doi.org/10.13182/NSE15-7.
102. R. T. SWEET et al., "Fuel Performance Simulation of Iron-Chrome-Aluminum (FeCrAl) Cladding During Steady-State LWR Operation," *Nucl. Eng. Des.*, **328**, 10 (2018); https://doi.org/10.1016/j.nucengdes.2017.11.043.
103. N. M. GEORGE et al., "Full-Core Analysis for FeCrAl Enhanced Accident Tolerant Fuel in Boiling Water Reactors," *Ann. Nucl. Energy*, **132**, 486 (2019); https://doi.org/10.1016/j.anucene.2019.04.025.
104. M. WAGIH et al., "Fuel Performance of Chromium-Coated Zirconium Alloy and Silicon Carbide Accident Tolerant Fuel Claddings," *Ann. Nucl. Energy*, **120**, 304 (2018); https://doi.org/10.1016/j.anucene.2018.06.001.
105. M. SEVECEK et al., "Development of Cr Cold Spray-Coated Fuel Cladding with Enhanced Accident Tolerance," *Nucl. Eng. Technol.*, **50**, *2, SI*, 229 (2018); https://doi.org/10.1016/j.net.2017.12.011.
106. K. A. GAMBLE, "Investigation of Coated Cladding Ballooning Behavior Using BISON," *Proc. TopFuel 2019*, Seattle, Washington, September 22–26, 2019.
107. P. G. MEDVEDEV and R. D. MARIANI, "Conductive Inserts to Reduce Nuclear Fuel Temperature," *J. Nucl. Mater.*, **531**, 151966 (2020); https://doi.org/10.1016/j.jnucmat.2019.151966.
108. A. A. REZWAN, M. R. TONKS, and M. P. SHORT, "Evaluations of the Performance of Multi-Metallic Layered Composite Cladding for the Light Water Reactor Accident Tolerant Fuel," *J. Nucl. Mater.*, **535**, 152136 (2020); https://doi.org/10.1016/j.jnucmat.2020.152136.
109. G. SINGH, K. TERRANI, and Y. KATOH, "Thermo-Mechanical Assessment of Full SiC/SiC Composite Cladding for LWR Applications with Sensitivity Analysis," *J. Nucl. Mater.*, **499**, 126 (2018); https://doi.org/10.1016/j.jnucmat.2017.11.004.
110. G. SINGH et al., "Parametric Evaluation of SiC/SiC Composite Cladding with UO_2 Fuel for LWR Applications: Fuel Rod Interactions and Impact of Nonuniform Power Profile in Fuel Rod," *J. Nucl. Mater.*, **499**, 155 (2018); https://doi.org/10.1016/j.jnucmat.2017.10.059.
111. G. SINGH et al., "Deformation Analysis of SiC-SiC Channel Box for BWR Applications," *J. Nucl. Mater.*, **513**, 71 (2019); https://doi.org/10.1016/j.jnucmat.2018.10.045.
112. G. SINGH et al., "Impact of Control Blade Insertion on the Deformation Behavior of SiC-SiC Channel Boxes in BWRs," *Nucl. Eng. Des.*, **363**, 110621 (2020); https://doi.org/10.1016/j.nucengdes.2020.110621.
113. G. K. MILLER et al., "Consideration of the Effects on Fuel Particle Behavior from Shrinkage Cracks in the Inner Pyrocarbon Layer," *J. Nucl. Mater.*, **295**, *2*, 205 (2001); https://doi.org/10.1016/S0022-3115(01)00551-7.
114. D. SCHAPPEL et al., "Modeling the Performance of TRISO-Based Fully Ceramic Matrix (FCM) Fuel in an LWR Environment Using BISON," *Nucl. Eng. Des.*, **335**, 116 (2018); https://doi.org/10.1016/j.nucengdes.2018.05.018.

115. R. L. SEIBERT et al., "Production and Characterization of TRISO Fuel Particles with Multilayered SiC," *J. Nucl. Mater.*, **515**, 215 (2019); https://doi.org/10.1016/j.jnucmat.2018.12.024.

116. D. SCHAPPEL et al., "Modeling Radionuclide Release of TRISO Bearing Fuel Compacts during Post-Irradiation Annealing Tests," *Nucl. Eng. Des.*, **357**, 110428 (2020); https://doi.org/10.1016/j.nucengdes.2019.110428.

117. D. SCHAPPEL, N. BROWN, and K. TERRANI, "Modeling Reactivity Insertion Experiments of TRISO Particles in NSRR Using BISON," *J. Nucl. Mater.*, **530**, 151965 (2020); https://doi.org/10.1016/j.jnucmat.2019.151965.

118. L. C. WALTERS, "Thirty Years of Fuels and Materials Information from EBR-II," *J. Nucl. Mater.*, **270**, *1–2*, 39 (1999); https://doi.org/10.1016/S0022-3115(98)00760-0.

119. J. I. SACKETT, "Operating and Test Experience with EBR-II, the IFR Prototype," *Prog. Nucl. Energy*, **31**, *1–2*, 111 (1997); https://doi.org/10.1016/0149-1970(96)00006-6.

120. G. L. HOFMAN et al., "Metallic Fuels Handbook," ANL-NSE-3, Argonne National Laboratory (1988).

121. S. R. NOVASCONE et al., "Summary and Assessment of Metallic Fuel Capabilities in Bison," INL/EXT-18-51399, Idaho National Laboratory (2018).

122. Y. MIAO et al., "Fuel Performance Evaluation of Annular Metallic Fuels for an Advanced Fast Reactor Concept," *Nucl. Eng. Des.*, **352**, 110157 (2019); https://doi.org/10.1016/j.nucengdes.2019.110157.

123. S. SEN et al., "A Versatile Coupled Test Reactor Concept," INL/CON-16-40086, Idaho National Laboratory (2017).

124. B. BEELER et al., "Atomistic Calculations of the Surface Energy as a Function of Composition and Temperature in Gamma U-Zr to Inform Fuel Performance Modeling," *J. Nucl. Mater.*, **540**, 152271 (2020); https://doi.org/10.1016/j.jnucmat.2020.152271.

125. J. KITTEL et al., "Properties of Fuels for Alternate Breeder Fuel Cycles," ANL-AFP-38, Argonne National Laboratory (1977).

126. H. SAVAGE, "The Heat Content and Specific Heat of Some Metallic Fast-reactor Fuels Containing Plutonium," *J. Nucl. Mater.*, **25**, *3*, 583 (1968); https://doi.org/10.1016/0022-3115(68)90168-2.

127. H. A. SALLER, R. F. DICKERSON, and W. E. MURR, "Uranium Alloys for High-Temperature Application," BMI-1098, Battelle Memorial Institute (1956).

128. D. R. OLANDER, "Fundamental Aspects of Nuclear Reactor Fuel Elements," Technical Information Center, Energy Research and Development Administration (1976).

129. R. G. PAHL et al., "Experimental Studies of U-Pu-Zr Fast Reactor Fuel Pins in EBR-II," CONF-8809202–2, Argonne National Laboratory (1988).

130. Y. ADDA, J. PHILIBERT, and H. FARAGGI, "Study of Intermetallic Diffusion Phenomena in Uranium-Zirconium System," *Rev. DeMetall.*, **54**, *8*, 597 (1957); https://doi.org/10.1051/metal/195754080597.

131. N. MÜLLER, "Diffusion Studies in the Uranium-Zirconium and Uranium-Nickel Systems," *Z. Metallk*, **50**, 652 (1959) (in German).

132. J. GALLOWAY et al., "Modeling Constituent Redistribution in U-Pu-Zr Metallic Fuel Using the Advanced Fuel Performance Code BISON," *J. Nucl. Mater.*, **286**, 1 (2015); https://doi.org/10.1016/j.nucengdes.2015.01.014.

133. M. F. MARCHBANKS, R. A. MOEN, and J. E. IRVIN, "Nuclear Systems Materials Handbook," HEDL-SA-871, Hanford Engineering Development Laboratory, Richland, Washington (1972).

134. F. GARNER and D. PORTER, "Irradiation Creep and Swelling of AISI 316 to Exposures of 130 dpa at 385–400C," *J. Nucl. Mater.*, **155**, 1006 (1988); https://doi.org/10.1016/0022-3115(88)90458-8.

135. "ASME Boiler and Pressure Vessel Code," Section II, Part D. 16Cr-12Ni-2Mo (Group 3), American Society of Mechanical Engineers (2019).

136. L. LEIBOWITZ and R. BLOMQUIST, "Thermal Conductivity and Thermal Expansion of Stainless Steels D9 and HT9," *Int. J. Thermophys.*, **9**, *5*, 873 (1988); https://doi.org/10.1007/bf00503252.

137. A. BANERJEE et al., "High Temperature Heat Capacity of Alloy D9 Using Drop Calorimetry Based Enthalpy Increment Measurements," *Int. J. Thermophys.*, **28**, *1*, 97 (2007); https://doi.org/10.1007/s10765-006-0136-0.

138. N. YAMANOUCHI et al., "Accumulation of Engineering Data for Practical Use of Reduced Activation Ferritic Steel: 8%Cr-2%W-0.2%V-0.04%Ta-Fe," *J. Nucl. Mater.*, 191–194, 822 (1992); https://doi.org/10.1016/0022-3115(92)90587-B.

139. "AFCI Materials Handbook, Materials Data for Particle Accelerator Applications, Chapter 18 — Design Properties of HT9 and Russian Ferritic/Martensitic Steels, Rev 6," LA-CP-14-20070, Los Alamos National Laboratory (2014).

140. T. H. BAUER, G. R. FENSKE, and J. M. KRAMER, "Cladding Failure Margins for Metallic Fuel in the Integral Fast Reactor," CONF-870812–22, Argonne National Laboratory (1987).

141. A. KARAHAN and J. BUONGIORNO, "A New Code for Predicting the Thermo-Mechanical and Irradiation Behavior of Metallic Fuels in Sodium Fast Reactors," *J. Nucl. Mater.*, **396**, *2 –3*, 283 (2010); https://doi.org/10.1016/j.jnucmat.2009.11.022.

142. C. JIANG et al., "CALPHAD Calculations of Lanthanide and Element Inter-Diffusion Between U-Zr Fuel and Steel Cladding," INL/EXT-19-55929 Rev. 0, Idaho National Laboratory (2019).

143. J. HIRSCHHORN et al., "A Study of Constituent Redistribution in U-Zr Fuels Using Quantitative Phase-Field Modeling and Sensitivity Analysis," *J. Nucl. Mater.*, **523**, 143 (2019); https://doi.org/10.1016/j.jnucmat.2019.05.053.

144. F. A. NICHOLS, "Theory of Columnar Grain Growth and Central Void Formation in Oxide Fuel Rods," *J. Nucl. Mater.*, **22**, *2*, 214 (1967); https://doi.org/10.1016/0022-3115(67)90031-1.

145. P. F. SENS, "The Kinetics of Pore Movement in UO_2 Fuel Rods," *J. Nucl. Mater.*, **43**, *3*, 293 (1972); https://doi.org/10.1016/0022-3115(72)90061-X.

146. A. KARAHAN, "Modeling of Thermo-Mechanical and Irradiation Behavior of Metallic and Oxide Fuels for Sodium Fast Reactors," PhD Thesis, Massachusetts Institute of Technology (2009).

147. T. OZAWA and T. ABE, "Development and Verifications of Fast Reactor Fuel Design Code CEPTAR," *Nucl. Technol.*, **156**, *1*, 39 (2006); https://doi.org/10.13182/NT156-39.

148. D. R. de HALAS and G. R. HORN, "Evolution of Uranium Dioxide Structure During Irradiation of Fuel Rods," *J. Nucl. Mater.*, **8**, *2*, 207 (1963); https://doi.org/10.1016/0022-3115(63)90036-9.

149. W. J. LACKEY, F. J. HOMAN, and A. R. OLSEN, "Porosity and Actinide Redistribution during Irradiation of $(U, Pu)O_2$," *Nucl. Technol.*, **16**, *1*, 120 (1972); https://doi.org/10.13182/NT72-A31181.

150. I. W. VANCE and P. C. MILLET, "Phase-Field Simulations of Pore Migration and Morphology Change in Thermal Gradients," *J. Nucl. Mater.*, **490**, 299 (2017); https://doi.org/10.1016/j.jnucmat.2017.04.027.

151. S. NOVASCONE et al., "Modeling Porosity Migration in LWR and Fast Reactor MOX Fuel Using the Finite Element Method," *J. Nucl. Mater.*, **508**, 226 (2018); https://doi.org/10.1016/j.jnucmat.2018.05.041.

152. J. M. HARP and H. J. M. CHICHESTER, "Baseline Postirradiation Examination of Fuel Rodlets from the AFC-2C Experiment," INL/MIS-17-42678, Idaho National Laboratory (July 2017).

153. W. L. OBERKAMPF and C. J. ROY, *Verification and Validation in Scientific Computing*, Cambridge University Press, Cambridge, United Kingdom (2010).

154. W. L. OBERKAMPF, M. PILCH, and T. G. TRUCANO, "Predictive Capability Maturity Model for Computational Modeling and Simulation," SAND2007-5948, Sandia National Laboratories (2007).

155. P. J. ROACHE, *Verification and Validation in Computational Science and Engineering*, Hermosa Publishing, Albuquerque, New Mexico (1998).

156. A. TOPTAN et al., "FY20 Verification of BISON Using Analytic and Manufactured Solutions," CASL-U-2020-1939-000, Consortium for the Advanced Simulation of Light Water Reactors (2020); https://doi.org/10.2172/1614683.

157. A. TOPTAN et al., "Construction of a Code Verification Matrix for Heat Conduction with Finite Element Code Applications," *ASME J. Verif. Validation Uncertainty Quantif*, **5**, 041002 (2020); https://doi.org/10.1115/1.4049037.

158. J. H. VAN SANT, "Conduction Heat Transfer Solutions," UCRL-52863-Rev.l; DE87 012387, Lawrence Livermore National Laboratory (1983); https://doi.org/10.2172/6224569.

159. Z. ALY et al., "Variance-Based Sensitivity Analysis Applied to the Hydrogen Migration and Redistribution Model in Bison. Part II: Uncertainty Quantification and Optimization," *J. Nucl. Mater.*, **523**, 478 (2019); https://doi.org/10.1016/j.jnucmat.2019.06.023.

160. E. R. BRADLEY, M. E. CUNNINGHAM, and D. D. LANNING, "Final Data Report for the Instrumented Fuel Assembly (IFA)-432," NUREG/CR-2567, PNNL-4240, Pacific Northwest National Laboratory (1982).

161. W. WIESENACK, *Halden Data Files for IFA-431 Rods 1, 2, and 3* (2012).

162. C. HANN et al., "Data Report for the NRC/PNL Halden Assembly IFA-432," NUREG/CR-0560, PNL-2673, Pacific Northwest Laboratory (1978).

163. W. WIESENACK, *Halden Data Files for IFA-432 Rods 1, 2, and 3* (2012).

164. T. TVERBERG and M. AMAYA, "Study of Thermal Behaviour of UO_2 and (U,Gd) O_2 to High Burnup (IFA-515)," HWR-671, Organisation for Economic Co-operation and Development Halden Reactor Project, Halden, Norway (2001).

165. J. A. TURNBULL, "Concluding Report on Three PWR Rods Irradiated to 90 MWd/kg UO_2 in IFA-519.9: Analysis of Measurements Obtained In-Pile and by PIE," HWR-668, Halden (2001).

166. "Fuel Modelling at Extended Burnup (FUMEX-II): Report of a Coordinated Research Project 2002–2007," IAEA-TECDOC-1687, International Atomic Energy Agency (2002–2007).

167. I. MATSSON, "The Effects of Grain Size on FGR and PCMI in High Burnup Fuel (IFA-534.14)," HWR-558, Halden (1999).

168. W. WIESENACK, *Halden Data Files for IFA-534 Rods 18 and 19* (2014).

169. "Improvement of Computer Codes Used for Fuel Behaviour Simulation (FUMEX-III): Report of a Coordinated Research Project 2008–2012," IAEA-TECDOC-1697, International Atomic Energy Agency (2008–2012).

170. G. ROSSITER, "IAEA FUMEX-III Co-ordinated Research Programme," Final Report NNL (12) 12172, National Nuclear Laboratory (2012).

171. P. LÖSÖNEN, "Early-in-Life Irradiation of IFA-562.2 (The Ultra High Burn-up Experiment)," HWR-247, Organisation for Economic Co-operation and Development Halden Reactor Project (1989).

172. I. MATSSON and J. A. TURNBULL, "The Integral Fuel Rod Behaviour Test IFA-597.3: Analysis of the Measurements," HWR-543, Halden (1998).

173. M. VANKEERBERGEN, "The Integral Fuel Rod Behaviour Test IFA-597.2: Pre-Characterization and Analysis of Measurements," HWR-442, Halden (1996).

174. T. TVERBERG, B. VOLKOV, and J. C. KIM, "Final Report on the UO_2-Gd_2O_3 Fuel Performance Test in IFA-636," HWR-817, Halden (2005).

175. "Data Sheet/IFA-677.1," QA-F-702, Organisation for Economic Co-operation and Development Halden Reactor Project (2005).

176. R. JOŠEK, "The High Initial Rating Test IFA-677: Final Report on In-Pile Results," HWR-872, Organisation for Economic Co-operation and DevelopmentHalden Reactor Project (2008).

177. H. K. JENSSEN, "PIE Report on Six UO_2Fuel Rods Irradiated in IFA-677 High Initial Rating Test," HWR-968, Organisation for Economic Co-operation and DevelopmentHalden Reactor Project (2010).

178. "The Risø Transient Fission Gas Release Project: Bump Tests with GE Fuel," Riso-TFGP-R10, Risø (1986).

179. "The Third Risø Fission Gas Project: Bump Test AN2 (CB6)," Risø-FGP3-AN2, Risø (1990).

180. "The Third Risø Fission Gas Project: Bump Test AN3 (CB8-2R)," Risø-FGP3-AN3, Risø (1990).

181. "The Third Risø Fission Gas Project: Bump Test AN4 (CB7-2R)," Risø-FGP3-AN4, Risø (1990).

182. "The Third Risø Fission Gas Project: Bump Test AN8 (CB10)," Risø–FGP3–AN8, Risø (1990).

183. "The Third Risø Fission Gas Project: Bump Test GE7 (ZX115)," Risø-FGP3-GE7, Risø (1990).

184. "The Third Risø Fission Gas Project: Bump Test II3 (STR014-3R)," Risø-FGP3-II3, Risø (1990).

185. "IFPE/OSIRIS R3 Database," Organisation for Economic Co-operation and Development, Nuclear Energy Data Bank (2002).

186. "IFPE/SPC-RE-GINNA Database," Organisation for Economic Co-operation and Development Nuclear Energy Data Bank (2002).

187. "Summary of the High Burn-up Effects Programme as Abstracted from the Programme Final Report," High Burn-up Effects Programme (2002).

188. "IFPE/Tribulation Database," Organisation for Economic Co-operation and Development Nuclear Energy Data Bank (2002).

189. M. E. MARKIEWICZ and F. ERBACHER, "Experiments on Ballooning in Pressurized and Transiently Heated Zircaloy-4 Tubes," KfK 4343, Kernforschungszentrum Karlsruhe (1988).

190. Z. HÓZER et al., "Ballooning Experiments with VVER Cladding," *Nucl. Technol.*, **152**, *3*, 273 (2005); https://doi.org/10.13182/NT05-A3676.

191. E. PEREZ-FERÓ et al., "Experimental Database of E110 Claddings Exposed to Accident Conditions," *J. Nucl. Mater.*, **397**, *1–3*, 48 (2010); https://doi.org/10.1016/j.jnucmat.2009.12.005.

192. E. PEREZ-FERÓ et al., "Experimental Database of E110 Claddings Under Accident Conditions," EK-FRL-2012-255-01/02, Center for Energy Research, Hungarian Academy of Sciences, Budapest, Hungary (2013).

193. D. HARDY, "High Temperature Expansion and Rupture Behaviour of Zircaloy Tubing," *CSNI Proc. of the Specialist Mtg. on Safety of Water Reactor Fuel Elements*, Saclay, France (1973).

194. C. P. MASSEY et al., "Cladding Burst Behavior of Fe-Based Alloys Under LOCA," *J. Nucl. Mater.*, **470**, 128 (2016); https://doi.org/10.1016/j.jnucmat.2015.12.018.

195. J. STUCKERT et al., "Results of the LOCA Reference Bundle Test QUENCH-L1 with Zircaloy-4 Claddings," KIT-SR 7651, Karlsruher Institut für Technologie (2015).

196. M. EK, "LOCA Testing at Halden; the Second Experiment IFA-650.2," HWR-813, Organisation for Economic Co-operation and Development Halden Reactor Project (2005).

197. F. B. DU CHOMONT, "LOCA Testing at Halden; the Ninth Experiment IFA-650.9," HWR-917, Organisation for Economic Co-operation and Development, Halden Reactor Project (2009).

198. A. LAVOIL, "LOCA Testing at Halden; the Tenth Experiment IFA-650.10," HWR-974, Organisation for Economic Co-operation and Development, Halden Reactor Project (2010).

199. F. SCHMITZ and J. PAPIN, "High Burnup Effects on Fuel Behaviour Under Accident Conditions: The Tests CABRI REP-Na," *J. Nucl. Mater.*, **270**, *1*, 55 (1999); https://doi.org/10.1016/S0022-3115(98)00895-2.

200. J. PAPIN et al., "Synthesis of CABRI-RIA Tests Interpretation," presented at the Eurosafe Forum, Paris, France, November 25–26, 2003.

201. J. PAPIN et al., "Summary and Interpretation of the CABRI REP-Na Program," *Nucl. Technol.*, **157**, *3*, 230 (2007); https://doi.org/10.13182/NT07-A3815.

202. B. THÉRACHE, "The High Initial Rating Test, IFA-677.1: Results After First Cycle of Irradiation," HWR-819, Organisation for Economic Co-operation and Development, Halden Reactor Project (2005).

203. O. BRÉMONT, "IFA-716.1 Fission Gas Release Mechanisms," HWR-1008, Organisation for Economic Co-operation and Development, Halden Reactor Project (2011).

204. T. TVERBERG, "Update on the In-Pile Results from the Fission Gas Release Mechanisms Study in IFA-716," HWR-1090, Organisation for Economic Co-operation and Development, Halden Reactor Project (2014).

205. B. BAURENS, "In-Pile Results from the Fission Gas Release Mechanisms Study in IFA-716 After Final Unloading," HWR-1161, Organisation for Economic Co-operation and Development, Halden Reactor Project (2016).

206. "Advances in High Temperature Gas Cooled Reactor Fuel Technology," IAEA-TECDOC-1674, International Atomic Energy Agency (2012).

207. T. H. BAUER et al., "First Overpower Tests of Metallic IFR Fuel in TREAT: Data and Analysis from Tests M5, M6, and M7," ANL-IFR-124, Argonne National Laboratory (1989).

208. L. GILPIN, R. BAKER, and S. CHASTAIN, "Evaluation of the Advanced Mixed Oxide Fuel Test FO-2 Irradiated in Fast Flux Test Facility," WHC-SA-0498, Westinghouse Hanford Co., Richland, Washington (1989).

209. M. KATO et al., "Physical Properties and Irradiation Behavior Analysis of Np- and Am-Bearing MOX Fuels," *J. Nucl. Sci. Technol.*, **48**, *4*, 646 (2011); https://doi.org/10.1080/18811248.2011.9711745.